Turun yliopisto
University of Turku

EMISSION, KINETIC AND MAGNETIC PHENOMENA IN RARE-EARTH AND TRANSITION METAL DOPED ZnSe SINGLE CRYSTALS

Ivan Radevici

TURUN YLIOPISTON JULKAISUJA – ANNALES UNIVERSITATIS TURKUENSIS
Sarja - ser. AI osa - tom. 515 | Astronomica - Chemica - Physica - Mathematica | Turku 2015

University of Turku

Faculty of Mathematics and Natural Sciences

Department of Physics and Astronomy

Wihuri Physical Laboratory

Supervised by

Prof. Petriina Paturi
Wihuri Physical Laboratory
Dept. of Physics and Astronomy
University of Turku
Turku, Finland

Prof. Dmitrii Nedeoglo
Dept. of Appl. Phys. and Comp. Science
Faculty of Phys. and Engin.
Moldova State University
Chisinau, Moldova

Dr. Hannu Huhtinen
Wihuri Physical Laboratory
Dept. of Physics and Astronomy
University of Turku
Turku, Finland

Reviewed by

Prof. Mircea Guina
Optoelectronics Research Centre
Tampere University of Technology
Tampere, Finland

Dr. Janusz Sadowski
MAX-IV laboratory
Lund University
Lund, Sweden

Opponent

Prof. Sergey Ivanov
Quantum-size Heterostructures Laboratory
Ioffe Physical-Technical Institute of RAS
26, Polytekhnicheskaya Str.
St.Petersburg 194021, Russia

The originality of this thesis has been checked in accordance with the University of Turku quality assurance system using the Turnitin OriginalityCheck service.

ISBN 978-951-29-6123-8 (PRINT)

ISBN 978-951-29-6124-5 (PDF)

ISSN 0082-7002

Painosalama Oy - Turku, Finland 2015

Physics is a collection of answers to some questions
that we put to the surrounding world.
And the world answers,
but with a condition that we will not question more...

Stanisław Lem

Preface

Acknowledgments

On the title page of this work there is written a single author name. Formally, this may be correct, but for me it feels to be a bit conceited. Even if not to think about all those, who spent their time teaching me some basic skills like reading, writing and computing (that is absolutely necessary to write a thesis, isn't it?), there are a lot of people, who directly helped me in many things related to this dissertation.

This work has been carried out in two institutions Wihuri Physical Laboratory of the Department of Physics and Astronomy at University of Turku and Department of Applied Physics and Computer Science of the Faculty of Physics and Engineering at Moldova State University. The Jenny and Antti Wihuri Foundation and Erasmus Mundus BMU-MID are acknowledged for generous financial support. I'm not sure if all the staff from this structures will read this acknowledgment (or even will know about it), but without your orginizing effort anything would not be done.

Also I would like to mention some names here, unfortunately not all because otherwise I'll need another tens of pages. I would like to express my deepest gratitude to Prof. P. Paturi whose knowledge, everyday optimism and efforts to arrange funding and opportunities to her students could not be over appreciated. I want to thank Prof. D. D. Nedeoglo, who motivated and helped me since my early undergraduate times and who is always available for a fruitful scientific (and not only) discussion. I could not omit Dr. H. Huhtinen, who always helped me with the unforeseen instrumental requirements or faults, and Dr. K. Sushkevich, who seems to know everything about semiconductor technology and crystal growth. Your critical opinion was very useful during all time of my work, especially during the time I were writing papers. I am very grateful to Prof. M. Guina and Dr. J. Sadowski for carefully reviewing my thesis and Prof. S. V. Ivanov for being my opponent — it is an honor.

I would like to thank my mom and (my mom's) mom for all they have done for me. Finally, I would like to thank (and sorry) everyone whose name flew out of my head just a couple of hours before sending this to the publishing house, but whose help is also included somewhere behind the cover.

Thank you all!!!

Turku, April 2015

not yet PhD Ivan Radevici

Abstract

In this work emission, optical, electrical and magnetic properties of the d- and f- elements doped zinc selenide crystals were investigated within a wide temperature range. Doping was performed in various technological processes: during the growth by chemical vapor transport method; by thermal diffusion from the Bi or Zn melt. Concentration of the doping impurity in the crystals was controlled by amount of the dopant in the source material or by its concentration in the doping media. Special interest in the work was paid to the influence of the different concentrations of Cr and Yb impurities on ZnSe crystals' properties, correlations between observed effects and similarities with the Ni, Mn and Gd dopants are analysed.

Possibility of formation of the excitons bound to the doping d-ions was shown. In contrast to this, it was observed that f-elements do not bound excitons, but prevent formation of excitons bound to some uncontrolled impurities. A mechanism of Cr doping impurity interaction with background impurities and zinc selenide structural defects was proposed based on experimental data. An assumption about resonant energy transfer between double charged chromium ions and complexes based on crystals' vacancy defects was made. A correlation between emission and magnetic properties of the d-ions doped samples was established. Based on this correlation a mechanism explaining the concentration quench of the emission was proposed.

It was found that f-ions bind electrically active shallow and deep donor and acceptor states of background impurity to electrically neutral complexes. This may be observed as "purification" of ZnSe crystals by doping with the rare-earth elements, resulting in tendency of the properties of f-ion doped crystals to the properties of intrinsic crystals, but with smaller concentration of uncontrolled native and impurity defects. A possible interpretation of this effect was proposed. It was shown that selenium substituting impurities decrease efficiency of the Yb doping. Based on this experimental results an attempt to determine ytterbium ion surroundings in the crystal lattice was made.

It was shown that co-doping of zinc selenide crystals with the d- and f- ions leads to the combination of the impurities influence on the material's properties. On the basis of obtained data an interaction mechanism of the d- and f-elements co-dopants was proposed. Guided by the model of the ytterbium ion incorporation in the selenide sublattice of the ZnSe crystals, an assumption about stabilization of single charged chromium ions in the zinc sublattice crystal nodes, by means of formation of the local charge compensating clusters, was made.

Tiivistelmä

Tässä työssä tutkittiin d- ja f-alkuaineilla doopattujen ZnSe-kiteiden emissio-, optisia, sähköisiä ja magneettisia ominaisuuksia laajalla lämpötila-alueella. Dooppaus tehtiin eri tekniikoilla: kasvatuksen aikana kemiallisesessa kaasufaasikasvatuksessa ja termisellä diffuusiolla Bi- tai Zn-nesteestä. Dooppauksen määrä kontrolloitiin säätämällä dopantin määrää lähtöaineissa tai sen konsentraatiolla dooppausnesteessä. Erityisesti tutkittiin Cr- ja Yb-atomien konsentraation vaikutusta ZnSe-kiteiden ominaisuuksiin sekä korrelaatioita havaittujen ilmiöiden välillä ja yhtäläisyyksiä Ni-, Mn- ja Gd-ioneilla doopattuihin kiteisiin.

Työssä osoitettiin, että d-ionien sitomien eksitonien syntyminen on mahdollista. Sen sijaan f-ionit eivät sido eksitoneja, vaan estävät niiden synnyn kontrolloimattomien epäpuhtausionien ympäristöön. Pohjautuen kokeelliseen dataan ehdotettiin, että resonoiva energian siirto Cr^{2+}-ionien ja kiteessä olevien vakanssien välillä selittää Cr-dopantin vuorovaikutuksen kontrolloimattomien epäpuhtausatomien kanssa. Työssä havaittiin myös korrelaatio magneettisten ja emissio-ominaisuuksien välillä d-atomeilla doopatuissa näytteissä ja tähän perustuen ehdotettiin mekanismia, joka selittää emission häviämisen dopantin konsentraation kasvaessa.

f-ionien havaittiin sitoutuvan kontrolloimattomien epäipuhtausatomien muodostamiin sähköisesti aktiivisiin mataliin ja syviin donori- ja akseptoritiloihin ja yhdessä ne muodostavat sähköisesti neutraaleja komplekseja. Tämän havaittiin näyttävän kiteen “puhdistumisena”, kun sitä doopataan harvinaisilla maametalleilla: kiteen ominaisuudet ovat yhä lähempänä täysin puhtaan ZnSe:n ominaisuuksia. Tälle ilmiölle esitettiin syntymekanismi. Työssä osoitettiin myös, että seleenin korvaavat epäpuhtaudet vähentävät Yb-dooppauksen tehoa. Tähän perustuen yritettiin määrittää Yb-ionien ympäristöä kidehilassa.

Työssä osoitettiin myös, että ZnSe-kiteiden dooppaaminen samanaikaisesti d- ja f-atomeilla johtaa dopanttien yhteisvaikutukseen kiteiden ominaisuuksissa. Kokeiden tuloksena ehdotettiin vuorovaikutusmekanismia dopanttien välille, jossa Yb-ionit korvaavat Se-ioneita Se-alihilassa ja samalla stabiloivat Cr^{+}-ioneita Zn-alihilassa muodostamalla paikallisia varauksen kompensoivia klustereita.

Glossary

ABE	acceptor bound exciton
CB	conduction band
CVT	chemical vapor transport
CW	continuous wave
DAP	donor-acceptor pair
DMS	diluted magnetic semiconductors
DPSSL	diode-pumped solid state lasers
ESR	electron spin resonance
FC	field-cooled
FE	free exciton
FWHM	full width at half maximum
IR	infrared
LO	longitudinal optical
OPO	optical parametric oscillators
PL	photoluminescence
PMT	photomultiplier tube
REE	rare-earth elements
RKKY	Ruderman–Kittel–Kasuya–Yosida
SA	self-activated
TM	transition metals
UV	ultraviolet
VB	valence band
ZFC	zero-field-cooled

μ	electron mobility
μ_F	Fermi energy
μ_F^*	reduced Fermi energy
μ	electron mobility
σ	electrical conductivity
σ_M	mass-magnetization
χ	magnetic susceptibility
A	acceptor center
D	donor center
e	electron or electron charge
E_A	acceptor energy
E_B	exciton bound energy
E_D	donor energy
E_g	bandgap energy
g	degeneracy factor
h	hole
J	effective coupling
k_B	Boltzmann constant
k_F	Fermi wavevector
M	volume magnetization
N_A	concentration of shallow acceptors
n_b	n in impurity band
n_c	n in conduction band
N_D	concentration of shallow donors
R_H	Hall coefficient

Articles included in this thesis

This thesis is based on the experimental work carried out at the Wihuri Physical Laboratory, Department of Physics, University of Turku during the years 2011 – 2014. The thesis consists of an introductory part and of the following publications:

[**P1**] I. Radevici, K. Sushkevich, G. Colibaba, V. Sirkeli, H. Huhtinen, N. Nedeoglo, D. Nedeoglo, P. Paturi: *Influence of chromium interaction with native and impurity defects on optical and luminescence properties of ZnSe:Cr crystals*, Journal of Applied Physics **114**, 203104 (2013).

[**P2**] V. Sirkeli, I. Radevici, K. Sushkevich, H. Huhtinen, N. Nedeoglo, D. Nedeoglo, P. Paturi: *Magnetic and luminescence properties of nickel-doped ZnSe crystals*, Solid State Sciences, (submitted).

[**P3**] I. Radevici, K. Sushkevich, H. Huhtinen, N. Nedeoglo, D. Nedeoglo, P. Paturi: *Magnetic and luminescence properties of chromium-doped ZnSe crystals*, Solid State Sciences **38**, 49 (2014).

[**P4**] I. Radevici, K. Sushkevich, H. Huhtinen, D. Nedeoglo, P. Paturi: *Influence of the ytterbium doping technique on the luminescent properties of ZnSe single crystals*, Journal of Luminescence **158**, 236 (2015).

[**P5**] I. Radevici, K. Sushkevich, V. Sirkeli, H. Huhtinen, D. Nedeoglo, P. Paturi: *Luminescent properties of the ZnSe:Yb crystals in the visible spectral range*, Journal of Luminescence **143**, 275 (2013).

[**P6**] I. Radevici, K. Sushkevich, V. Sirkeli, H. Huhtinen, N. Nedeoglo, D. Nedeoglo, P. Paturi: *Purification of ZnSe from electrically active background impurities by Yb doping*, Physica Status Solidi (b) **251**, 1565 (2014).

[**P7**] I. Radevici: *Influence of the chromium and ytterbium co-doping on the photoluminescence of zinc selenide crystals*, Journal of Rare Earths **32**, 938 (2014).

Articles relevant to this work but not included in this thesis

[**P8**] L. Kulyuk, R. Laiho, A. Lashkul, E. Lähderanta, D. Nedeoglo, N. Nedeoglo, I. Radevici, A. Siminel, V. Sirkeli, K. Sushkevich: *Magnetic and luminescent properties of iron-doped ZnSe crystals*, Physica B **405**, 4330 (2010).

[**P9**] J.-P. Biethan, H. Hartnagel, R. Laiho, A. Lashkul, E. Lähderanta, D. Nedeoglo, N. Nedeoglo, D. Pavlidis, I. Radevici, V. Sirkeli, R. Sobolevskaia, K. Sushkevich, O. Yilmazoglu: *Magnetic and luminescent properties of manganese-doped ZnSe crystals*, Physica B **407**, 3802 (2012).

Contents

1 Introduction

1.1 Semiconductors

Optoelectronics brings together optics and electronics within a single device, a single material. The material of choice needs to allow the manipulation of light, the manipulation of electrical current, and their interaction. Metals are excellent electrical conductors, but do not allow light to propagate. Glass and related dielectric materials can accommodate and guide light waves, but they are electrical insulators. Semiconductors are in between these two material types, as they can carry electrical current as well as light waves. Even better, semiconductors can be designed to allow for the transformation of light into current and vice versa.

The conduction of electrical current is based on the flow of electrons. Most electrons are bound to single atoms and do not transport charge. Only some electrons on the external shells are released and become conduction electrons. The same number of positively charged ions is left. The positive charges can also move, as valence electrons move from atom to atom. Both groups of valence electrons (holes) and conduction electrons are able to carry electrical current. Both types of carriers are separated by an energy gap; i.e., valence electrons need to receive at least the gap energy E_g to become conduction electrons (Fig. 1).

To control the concentration of electrons or holes, impurity atoms are introduced into the semiconductor crystal. The dopants have energy levels slightly above the valence band (VB), acceptors, or slightly below the conduction band (CB), donors (Fig. 1). Acceptors receive an additional electron from the valence band and become negatively charged ions, thereby generating a hole (p-doping). Donors release an electron into the conduction band and become positively charged ions (n-doping) [1]. Donor and acceptor impurities may be divided into two groups: deep and shallow. Characteristic for the last group is determination of the energy levels by the core's long range coulomb potential, for the deep donors or acceptors energy levels are defined by the core's short range potential. Usually shallow impurity levels differ less than hundred meV from the allowed band edges, while deep levels are placed closer to the middle of the bandgap.

Thus, semiconductor is a material with intermediate conductivity between metals and dielectrics, which is strongly dependent on the crystal structure, impurities and external conditions, i.e., temperature, illumination, electric or magnetic field etc.

There are several classification of semiconductor materials: by type of conductivity semiconductors can be intrinsic or extrinsic. The last group divides into n-type and p-

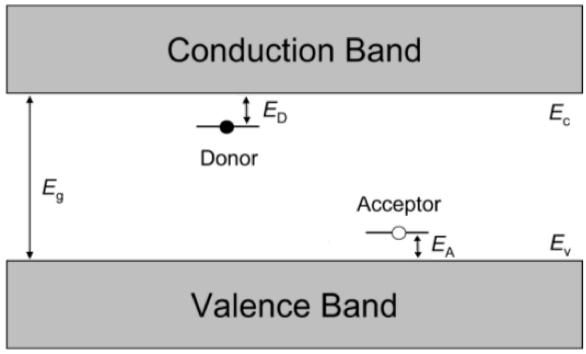

Figure 1: Illustration of donor and acceptor levels within the energy bandgap (E_D and E_A are activation energies).

type. By composition elementary (e.g. Si, Ge), binary (e.g. GaAs, CdTe), ternary (e.g. $CuInSe_2$), etc. Binary semiconductor compounds include several groups depending on the component elements: II-VI compounds (e.g. CdTe, ZnS), III-V compounds (e.g. GaAs, InN), IV-VI compounds (e.g. PbTe, SnS), etc. Semiconductors formed by the elements of II and VI groups of the periodic table have been known for a relatively long time. Their properties, like high photosensitivity, high probability of emission recombination in the case of direct transitions and large bandgap, are used in many practical applications [2]. However, the well-known problems of near-equilibrium doping and self-compensation must be overcome for the wider use of the wide-bandgap II–VI compounds in industry [3].

1.2 Luminescence

The notion of luminescence was introduced by Eilhard Wiedemann in 1888. According to this definition luminescence (from latin "lumen": light) is the "light emission predominant over the background thermal noise, i.e., emission not conditioned by the rise in temperature" (not incandescence) [4]. However, the Wiedemann's definition is too wide and includes all types of non-equilibrium emission including, e.g., Rayleigh and Raman. To separate luminescence from another emission types Sergey Vavilov introduced the lifetime criteria. Thus, the contemporary definition of luminescence is a spontaneous emission of radiation from an electronically excited states not in thermal equilibrium with its environment, and duration of the overglow more than half-period of the light oscillation [5].

Table 1: Types of luminescence.

Designation	Excitation	Trigger	Acronym
Photoluminescence	Photons	-	PL
Radioluminescence	X-ray, gamma rays, charged particles	-	RL
Cathodoluminescence	Energetic electrons	-	CL
Electroluminescence	Electric field	-	EL
Thermoluminescence	Photons, charged particles	Heat	TSL
Bioluminescence	Biochemical reaction	-	BL
Chemiluminescence	Chemical reaction	-	CHL
Triboluminescence	Strain, fracture	-	TL
Sonoluminescence	Sound wave	-	SL

Luminescence as a process may be conventionally divided into three stages: excitation or ionization of the emission centers, their stay in the excited or ionized state, and the light emission. On the first stage, a wide range of energy sources can stimulate luminescence, and their diversity provides a convenient classification scheme for luminescence phenomena (see Table 1). On the second stage of luminescence, when the emission centers are in the excited state, diffusion of the non-equilibrium charge carriers and their interaction with ionized emission centers take place. The third stage of luminescence may be divided into either intrashell (monomolecular) or recombination emission. In the first case luminescence appears because of transition of the earlier excited center to the equilibrium state. In the last one emission is caused by recombination of different charge carriers [6].

Photoluminescence (PL), where the luminescence is most often stimulated by ultraviolet (UV) or visible light, is a frequently used technique in materials science for characterising dopants and impurities. For example, PL in semiconductors is dominated by near-bandgap luminescence arising from recombination of free electrons and holes. This process has the highest efficiency in direct-bandgap materials such as ZnSe and GaP lower in indirect-gap materials (e.g. Si and Ge) because the transition probability requires conservation of wavevector. The photon wavevector is ≈ 0 on the scale of the Brillouin zone. Thus, creation or destruction of a phonon is needed for band-to-band luminescence in indirect-gap materials, which is less probable. The term edge luminescence is applied to a recombination processes leading to appearance of photons with energy of few tenth of eV smaller than the E_g. The edge luminescence arises from

a variety of shallow energy-level structures such as free or bound excitons [2].

The deep-level luminescence is a particular case of the recombination emission that appears at longer wavelengths than the edge luminescence. There are three main mechanisms for this type of emission. The Klasens model represents recombination of the free major charge carriers with localized minor charge carriers. Particularity of this recombination scheme is correlation between the photoinduced current and emission intensity [7]. The Lambe-Klick model may be applied to the recombination of the free minor charge carriers with localized major charge carriers [8]. The Prener-Apple-Williams scheme assumes emission recombination within an interactive donor-acceptor pair (DAP) [9].

1.3 Impurity band

It was observed that at some relatively high doping impurity concentrations in semiconductors the Hall coefficient and the resistivity do not increase indefinitely with decreasing temperature, as predicted by the usual theory. Thus, the absolute value of the Hall coefficient goes through maximum at low temperatures, but the resistivity approaches a saturation. This anomaly in both the resistivity and the Hall effect requires a modification of the usual theory of an extrinsic semiconductor with localized impurity states [10]. The Hall coefficient may decrease from its maximum by a factor of over 100 as the temperature is decreased. The concentration of free carriers in the conduction band (or the other filled band), on the other hand, can not be expected to increase with decreasing temperature. This allows to conclude that the usual expressions for electrical conductivity σ and Hall coefficient R_H

$$\sigma = en\mu, \tag{1}$$

$$R_H = \frac{1}{ne}, \tag{2}$$

can not be applied at low temperatures [11]. Here n is the free electron concentration, e is an electron charge, and μ is electron mobility. The experimentally observed results can be explained only if a mechanism is found that includes a combination of different kinds of charge carriers with various mobilities. James and Ginzbarg [12] assumed that due to the interaction between the impurity states, an impurity band is formed.

Basing on James and Ginzbarg model, an impurity band forms by the interaction of localized impurity states, in other words by the overlapping of their wave functions. The energy distribution of states in a perfect crystal is not the same as that of a crystal in which n-type impurity atom substitutes a regular lattice atom. In the latter case

the difference consists in absence of two energy states from the conduction band and one energy state (doubly degenerate) appears in the forbidden gap. The degeneracy is caused by the alternative spin directions. The corresponding eigenfunctions should be localized, thus, they have a finite amplitude only near the impurity. If there are two impurities replacing regular lattice atoms, than two doubly-degenerate energy states rise in the semiconductor bandgap and a similar number of states disappears from the conduction band. The difference in energy between the mentioned states can be obtained in terms of an exchange integral of the single-impurity wave functions. The eigenfunctions of these energy states may also be appreciated only in the neighborhood of the two impurities. When there are many impurities, the group of energy states in the forbidden energy gap is called an impurity band.

In the hypothetical case when impurity atoms are periodically arranged, the impurity band is separated from the lowest energy level in the conduction band (or from the highest energy level in the valence band in p-type) by a forbidden gap. This contains twice of energy states as there is number of impurity atoms. James and Ginzbarg have proofed that, if the case of random distribution of impurities the impurity band represents an energy range of high-level density, distanced from the conduction band by a range of smaller level density and the number of energy states in the impurity band is twice less comparing to the number of impurity atoms [13].

When simultaneous conduction in both the donor band and the conduction band (or the acceptor band and the filled band) can not be neglected, the expressions for conductivity σ and the Hall coefficient R_H are given as follows:

$$\sigma = en_c\mu_c + en_b\mu_b, \tag{3}$$

$$R_H = \frac{en_c\mu_c^2 + en_b\mu_b^2}{(en_c\mu_c + en_b\mu_b)^2}, \tag{4}$$

where n_b and μ_b are the concentration and mobility of charge carriers in the impurity band, and n_c and μ_c are the concentration and mobility of charge carriers in the conductance band.

Since μ_b has usually smaller value than μ at high temperatures, the conduction within the impurity band can be neglected. Thus values of σ and R_H may be obtained from Eqs. (1) and (2) with respect to the usual theory. At the decreasing temperature n decreases indefinitely, conduction within the impurity band increases and becomes important, so at low temperatures conduction in the conduction band can be neglected. At sufficiently low temperatures, all the charge carriers are in the impurity band, and at room temperature, all the electrons are excited into the conduction band. Therefore, the

Hall coefficients at room temperature and at very low temperatures have similar value. At intermediate temperatures both contribution should be taken into account. This is in approximate agreement with experiment [11].

1.4 Magnetism

The origin of magnetism lies in the orbital and spin motions of electrons and how the electrons interact with each other. The fundamental object in magnetism is the magnetic moment, equivalent to a current loop in classical electromagnetism. A magnetic solid consists of a large number of atoms with magnetic moments. The quantitative description of the magnetic properties of a solid is given by magnetization M, defined as the magnetic moment per unit volume, or mass-magnetization σ_M, representing magnetic moment per unit mass. In the special case when the magnetization M is linearly related to the magnetic field H and may be represented as $M = \chi H$, where χ is proportionality coefficient named magnetic susceptibility. The definition of M means that χ represents the magnetic moment induced by a magnetic field H per unit volume, however, it may be reformulated for the unit mass (mass susceptibility) or molar volume (molar magnetic susceptibility). Depending on reaction of the material to the external magnetic field materials may be classified.

In diamagnetic substance, a magnetic field induces a magnetic moment which opposes the applied magnetic field that caused it. This effect is often discussed from a classical viewpoint: the action of a magnetic field on the orbital motion of an electron causes a back electromotive force, which by Lenz's law opposes the magnetic field which causes it. Paramagnetism corresponds to a positive susceptibility so that an applied magnetic field induces a magnetization, which aligns parallel with the applied magnetic field which caused it. Magnetic moments of atoms that do have a non-zero magnetic moment without an applied magnetic field point in random directions because the magnetic moments on neighbouring atoms interact only very weakly with each other and can be assumed to be independent. The application of a magnetic field lines them up, the degree of lining up (and hence the induced magnetization) depends on the strength of the applied magnetic field. Unlike two previous cases interaction between magnetic moments in ferromagnetic and antiferromagnetic materials is very strong leading to parallel and antiparallel orientation, respectively, of the magnetic moments in the external field [14].

Materials based on II-VI semiconductor compounds in which a fraction of the non-magnetic cations (e.g. Zn^{2+}) has been randomly replaced by magnetic ions (e.g. Cr,

Fe, Eu), are widely known as diluted magnetic semiconductors (DMS) [15]. DMSs form two distinct classes. The first class consists of materials, in which the presence of robust ferromagnetism correlates with the existence of nanoscale regions containing a large density of magnetic cations. These regions represent condensed magnetic semiconductors buried in the host matrix and specified by a high spin ordering temperature. The second class of ferromagnetic DMSs comprises semiconductors containing randomly distributed magnetic impurities. In these materials charge carriers can mediate efficient long-range ferromagnetic spin-spin couplings.

There are 5 main mechanisms of the exchange interaction in DMS. The potential and kinetic exchange interactions represent spin exchange mechanisms. The superexchange interaction caused by either attraction or repulsion by the adjacent magnetic ions of the charge carriers, depending on the mutual orientation of the itinerant and localized spins. This results in a spatial redistribution of spin-down and spin-up valence band electrons. The Ruderman–Kittel–Kasuya–Yosida (RKKY) model is based on carrier-mediated interaction between localized spins and its value oscillates with the distance between these localized states as

$$F(\xi) = (\sin\xi - \xi\cos\xi)/\xi^4, \tag{5}$$

where $\xi = 2k_F r$, k_F being the Fermi wavevector and r the distance between magnetic impurities [16]. The double exchange mechanism operates if the width of a partly occupied band is smaller than the energy of the exchange interaction of carriers with localized spins. This situation occurs if magnetic ions with differing charge states coexist. The Stoner ferromagnetism occurs when an overlap between transition metals (TM) d orbitals leads to a Mott–Hubbard insulator-to-metal transition [17].

The interest in DMS is primarily a result of their unique features: the existence of magnetic phenomena in a host with a simple band and crystallographic structure; the possibility of reliable control of stoichiometry as well as of carrier, impurity, and magnetic-ion concentration; excellent optical and transport properties enabling application of the most powerful methods that have been developed for the studies of canonical semiconductors [18].

1.5 d- and f-element dopants

It has been known for a long time that the influence of impurity atoms on material magnetic and emission properties is ultimately related to the position of the energy levels with respect to the Fermi level and band edges. This position as well as the ion

charge state, and the nature of the excited states are determined by various competing interactions [18]. A wide variety of centers gives rise to luminescence and magnetism in semiconductors and insulating materials, including rare-earth elements (REE) and TM ions. Luminescence spectra of TM doped materials includes broad emission bands caused by the interaction between the charge carriers localised at the luminescent center and other particles (including phonons) which surround it. Bands may arise from simultaneous transitions of electronic as well as vibrational systems. For REE materials the spectra consist of sharp lines coming from purely electronic transitions. In this case the effect of the REE environment is reduced to change of the lifetimes of the states. Thus the physical background to luminescence and magnetism is simpler for the REE impuritites, where the effect of vibrations can be ignored [6].

The triply charged rare-earth ion has n electrons (n = 1 - 14) in the $4f$ shell. In the case of a free ion, the eigenstates rised from the various atomic interactions are distinguished by the total spin S and orbital angular momenta L. Spin-orbit coupling breaks each L, S multiplet of degeneracy $(2S + 1)(2L + 1)$ into sub-multiplets marked by the total angular momentum $J = L + S$, where J can range from L - S to $L + S$. The $4f^n$ orbitals lie within the outer $5s^2$ and $5p^6$ filled shells. These are partly shielded from the effects of the crystalline environment. The crystal-field splitting is smaller than the spin–orbit splitting. Thus, the multiplet labels follow the usual $^{2S+1}L_J$ system [18].

Study of the REE doped semiconductors is interesting form both the fundamental and application points of view. For example, the interaction between REE ion $4f$-electrons with the free charge carriers or bulk crystal lattice recombination center electrons presents a particular interest. Absence of the free charge carriers in the pure ionic crystals allows to presuppose that such effects may be observed only in II-VI semiconductor compounds [19]. This context has significantly stimulated research on the optical and magnetic properties of the wide bandgap semiconductors doped with f- element ions [19–23]. Photo- [24, 25] and electroluminescence [26], excitation spectra, optical absorption [27] and electron spin resonance (ESR) [28–30] have been studied. Results of the last allowed to determine the possible sites of the REE ion in the bulk crystal lattice and its surrounding, as well as energy transfer mechanisms between REE ion and Li, Cu, Ag ions [31–33]. While the REE chalcogenides were among the most studied magnetic semiconductors, there have been only a few reports on DMS incorporating REE as the magnetic constituent. Such a situation has largely been caused by the low solubility limit of the rare earths in both III-V and II-VI semiconductor compounds as well as by their tendency to form clusters and to occupy other sites than the cation

substitutional ones [18].

For example, Brown et al. [32] have described a center formed by the triply charged REE substituting the anion and surrounded by a tetrahedron of cations. Charge compensation for this type of center is provided by formation of a cluster, which includes the studied rare-earth ion and background impurities. However, many other centers formed by a REE ion have been described. A substitutional one, when REE is placed in the cation node and 4 first order neighbors, anions, are on their places as they would be in the ideal crystal [28, 31]. Calculated values for this model are unexpectedly close to the experimental values [29]. Another center may exist, when the dopant ion is placed in an interstitial site and the crystal lattice is deformed. In this case, the closest neighbors, 4 cations and 6 anions, are displaced in such a way that they compensate local charge disbalance, caused by incorporation of the triply charged REE ion. Charge compensation may be also achieved by replacing double charged cations in the crystal lattice nodes with single charged ions of the another (compensating) impurity. This leads to formation of a cluster, which does not change the local charges and does not deform the lattice.

Transition metals from the $3d$ series have a much stronger interaction with the crystal lattice comparing to the $4f$ ions since there is no equivalent to the screening outer shells ($5s$, $5p$). Also, the spin–orbit coupling is weaker, so the order of perturbation is reversed: the atomic L, S multiplets are split by the crystal field, with spin–orbit coupling being a smaller interaction. Intra-configurational transitions are again strictly forbidden, but become weakly allowed by inter-configurational mixing through odd-parity crystal fields, and by odd-parity vibrations. This results in the strongest selection rule after parity, thus, transitions should have $\Delta S = 0$ (the electric dipole operator does not involve spin). Abother difference is caused by the strength of the crystal-field interaction. Transitions thar are purely electronic (zero-phonon lines) are rarely observed [6]

Despite the fact, that all TM ions isoelectronically replace cations in II-VI semiconductor compounds (e.g. [34, 35]) and do not form complexes, the experimental results on their magnetic and emission properties are ambiguous and often contradictory. For example, it was considered that Cr-based DMS should reveal an intermediate magnetic behaviour between Brillouin-type paramagnetism, resulting from the single multiplet ground state of the doping ion (e.g. Mn or Co), and Van Vleck-type paramagnetism, due to the singlet ground state of the TM (e.g. Fe) [36]. This behaviour was experimentally confirmed [37], however, there are other experimental data, which

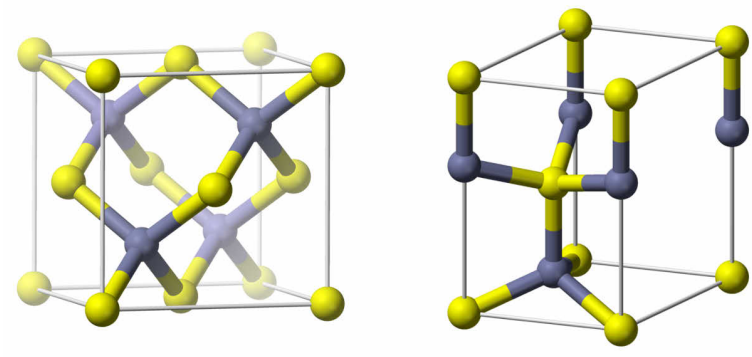

Figure 2: The unit cell of zinc blende (left side) and wurtzite (right side) crystals structure.

reveal antiferromagnetic [38] and ferromagnetic [39] behaviour of the chromium doped II-VI compounds. A similar contradiction appears in determination of the maximum position of the chromium intrashell emission: 1.8 μm (0.67 eV) [40], 2.1 μm (0.59 eV) [41, 42], 2.2 μm (0.56 eV) [43], 2.4 μm (0. 51 eV) [44, 45].

1.6 ZnSe

Zinc selenide is a binary diamond type wide bandgap semiconductor (E_g(300K) = 2.722 $\pm$ 0.003 eV, E_g(5K) = 2.820 eV [46]). It is a part of both Ge-GaAs isoelectronic series and II-VI semiconductor compounds group [47]. It is empirical rule that the behavior of bond energy versus covalency is quite linear in the isoelectronic series, thus, is a series of compounds with the similar electron density [46]. This results in similarity of electrical properties of the ZnSe crystals with electrical properties of such largely used materials as GaAs. On the other hand, ZnSe as a wide bandgap II-VI compound has a high transparency in both visible and infrared (IR) spectral ranges, good stability to commonly used chemical reagents and also industry-acceptable thermal and mechanical properties. All these make zinc selenide an ideal candidate for optoelectronic applications. Thus, ZnSe is a valuable model material for both Ge-GaAs isoelectronic series and II-VI semiconductors group. Main properties of ZnSe required for practical applications are listed in Table 2.

Depending on the growth conditions ZnSe may form sphalerite (zincblend) or wurtzite structure (Fig. 2). The first one represents a cubic crystal cell from the hextetrahedral crystallographic class (space group F$\bar{4}$3m). Every Zn(Se) atom is surrounded with

Table 2: Properties of zinc selenide used in laser (LASERTRAN) and infrared (INFRATRAN) optics [48].

Material	**LASERTRAN**	**INFRATRAN**
Absorption coefficient at 10.6 μm, cm^{-1}	$< 5 \cdot 10^{-4}$	$< 7 \cdot 10^{-3}$
Characteristic transmission at 10.6 μm for 6-mm-thick samples, %	> 99.97	> 99.9
10% transmission range, μm	> 0.5-22	
Pulsed CO_2 laser damage threshold, J/cm^2	> 20	Not standardized
Refractive-index nonuniformity at 0.6328 μm	$< 5 \cdot 10^{-6}$	Not standardized
Inclusions	No observable inclusions	Inclusions less than 100 μm in size may be present
Melting point, °C	1520 ± 15	
Thermal expansion coefficient, K^{-1}	$7.6 \cdot 10^{-6}$	
Mean grain size, μm	50 - 70	
Bending strength, MPa	50	
Knoop hardness, MPa	1500	

4 Se(Zn) atoms placed in the vertices of a regular tetrahedron on a distance of $1/4\sqrt{3}a$, where a is a lattice constant 5.668 Å [46], 12 atoms of the same type, each placed at $1/2\sqrt{2}a$, are the second order neighbors. The wurtzite structure is hexagonal (the space group $P6_3mc$). The lattice constants for the ZnSe wurtzite modification are a = 4.003 Å and c = 6.540 Å [46].

Both structures are very similar, thus the crystal grown from the vapor phase may form politypes: combination of both cubic and hexagonal structures. It is known that excess of Se during the crystal growth leads to formation of cubic modification and to modification of the hexagonal structure to the cubic one. Opposite to this, excess of Zn leads to stabilization of the hexagonal phase. However, crystals with just wurtzite structure may be obtained only by hydrazine reduction of the zinc selenite [49]. The shortest distance between the different atoms is d(Zn-Se) = 2.45 Å, and between similar is d(Zn-Zn) = 4.01 Å. It is also worth mentioning that the ionic radius of major d- and f-elements is smaller than ionic radius of zinc (e.g. $r(Zn^{2+})$ = 0.74 Å, $r(Cr^{2+})$ = 0.73

Å, $r(Ni^{2+})$ = 0.69 Å, $r(Yb^{3+})$ = 0.87 Å) this favors doping of ZnSe with TM and REE elements. However, the selenium ionic radius is much bigger ($r(Se^{2-})$ = 1.98 Å), which does not exclude formation of antisites [50].

1.7 Motivation

Infrared lasers tunable in wide spectral range have found their applications in many fields: acousto-optical gas detection and determination of gas concentrations, environment monitoring, electronic communications, as well as numerous medical or military applications [51–53]. Obtaining tunable emission in IR spectral range is possible using, for example, optical parametric oscillators (OPO), which may generate electro-magnetic waves in a range from UV to mid-IR spectral region [54]. OPO's main disadvantages are large dimensions and high price. Usage of quantum cascade lasers may be a good alternative to OPO, but they may function only at low temperatures, their production is extremely expensive and tunability range is narrow [55]. These factors attracted attention to development of diode-pumped solid state lasers (DPSSL) on the base of Zn and Cd chalcogenides doped with TM, for example, Cr^{2+} and Fe^{2+}. Despite a smaller tunability range, comparing to OPO, these lasers have many advantages, like low production cost, room-temperature functioning, flexible pulse format modes [45, 54] also their electrical pumping may be developed [51, 56].

One of the most studied TM doped zinc chalcogenides is ZnSe:Cr. Spectroscopic properties of this material are: 1) quantum efficiency close to one at room temperature, 2) wide absorption band near 1.8 μm, which allows optical pumping of intra-shell transitions with various methods and 3) absence of significant absorption on the excited state in mid-IR spectral range [51, 57], make it a valuable source of coherent emission in the mid-IR spectral range. Intensive study of ZnSe:Cr crystals allowed not only to determine the structure of the doping impurity energy levels [58], their optical [59, 60] and luminescent [59] properties, but also to elaborate few prototypes of the laser system working in pulsed [61] and continuous modes [62].

The interest in the materials doped with REE is also renewed in the last few years. This is mainly caused by various practical applications, where such materials may be used. The emission properties of the REE ions have attracted particular interest [63, 64]. It has been shown that REE-doped garnets are efficient active media for the DPSSL [65, 66], self-Q-switched Er/Yb fiber lasers are developed for use in telecommunications [67, 68], and REE-doped glasses are promising for eye-safe applications in medicine and meteorology [69]. Recently, a new potential application has emerged: the use of

II-VI semiconductors doped with lanthanide ions for spectral conversion in solar cells to reduce the spectral mismatch losses [70].

Particular interest to Yb^{3+} ion is caused by its relatively simple energy diagram (electronic structure of $[Xe]^4 f^{13}$ type), presented by one excited state $^2F_{5/2}$ and a ground $^2F_{7/2}$ state lying $\sim$1.2 eV below, absence of the line widening and absorption on the excited state [32, 71]. The extremely simple energy structure of the Yb^{3+} ion allows to use it as a model for other REE ions. However, a possible resonance energy transfer between ytterbium and TM dopants [72] stimulates a practical interest to Yb-doped materials.

Historically, the magnetism of doped wide bandgap semiconductors and their optical properties have been considered separately in relation to different tasks. However, DMS, which combine both magnetic and optical properties, seem to be the most novel and interesting objects for investigation not only because of their fundamental properties (e.g. giant Faraday rotation or giant exciton splitting) [73], but also because of their practical applications in magneto-optics and magneto-electronics [74, 75]. In this thesis, the complex investigation of the TM and REE doping effects on electric, magnetic and luminescent properties of the zinc selenide crystals. Special interest will be paid to the influence of the Cr and Yb impurities concentrations on ZnSe crystals' properties, correlations between observed effects and similarities with the Ni and Gd dopants will be analysed.

2 Experimental details

2.1 Sample preparation

The ZnSe crystals doped with Cr, Ni, Yb and Gd were studied in this thesis. The doping was performed during the crystal growth from elements or by the thermal diffusion from melt. Growth and diffusion conditions were similar for all the studied crystal series. Impurity concentration used further in the thesis corresponds to the dopant concentration in the source material for growth or in the annealing media.

The chemical vapor transport (CVT) method with iodine as transportation agent was used for the doping of the ZnSe crystals during the growth process. The growth technique is based on interaction of a gaseous agent A with a non-volatile substance X (material for the crystal growth). Depending on external conditions (temperature and partial pressures) formation of various gaseous molecules of the A_pX_d type takes place. Change of the these external conditions may lead to decomposition of the volatile compound with separation of the substance X. Thus, for the crystallization of X, it is necessary to create a temperature gradient and to place in it the source material X and the transportation agent. In this case at some temperature T_1 in the source zone formation of the volatile molecules A_pX_d will take place, and in the growth zone these molecules will decompose at T_2. After the decomposition the transportation agent should diffuse back into the source zone. Thus a fixed amount of the transportation agent may provide crystallization of arbitraty amount of the substance X [76]. Reaction used for the growth of ZnSe crystals may be written as

$$2\mathrm{ZnSe}_{(solid)} + \mathrm{I}_{2(gas)} \rightleftharpoons 2\mathrm{ZnI}_{2(gas)} + \mathrm{Se}_{2(gas)}. \quad (6)$$

Choice of the reaction (6) is based on the following: reaction is heterogeneous (solid substance is presented only in one part of reaction, this guarantees the transport); in equilibrium conditions (in absence of a temperature gradient) the reaction does not lead to any significant transport of the substance; reaction is thermo-chemical (formation of gaseous agent is endothermic, thus, takes place with heat absorption, crystallization reaction is exothermal) allowing to control it on the basis of Le Châtelier's principle (transport goes from the zone with higher temperature to the zone with lower temperature) [48, 77].

Crystallization process may be divided into the few stages. On the first stage a volatile compound (ZnI_2) forms in the zone with higher temperature. Concentration gradient leads to transport of this compound into the zone with lower temperature. TM

and REE dopant is also transported by the transportation agent. It should be mentioned that in the case of ZnSe chalcogen is not transported by the agent, selenium forms diatomic molecule, which moves to the crystallization zone by itself. On the second stage the decomposition of the volatile compound takes place, and solid compound crystallizes in the growth zone. On the last stage diatomic molecule of the transportation agent (I_2) moves back to the source zone.

The number of atoms is proportional to the amount of substance, thus, the masses of substances for the growth process may be determined from the following: $m(\text{Zn}) = (1-C')\cdot\nu\cdot M(\text{Zn})$; $m(X) = C'\cdot\nu\cdot M(X)$; $m(\text{Se}) = \nu\cdot M(\text{Se})$, where X is the doping impurity, C' is concentration of the dopant in unity fractions, ν is amount of substance calculated from the needed crystal's mass, $m(\text{Zn})$, $m(X)$, $m(\text{Se})$ are the masses of zinc, dopant and selenium, respectively, in the source zone; $M(\text{Zn})$, $M(X)$, $M(\text{Se})$ are the molar weights of zinc, dopant and selenium, respectively. Transformation of concentration units may be done as follows: $C[\text{at.}\%] = 100 \cdot C'$ and $C[\text{cm}^{-3}] = N_A \cdot \rho(\text{ZnSe})\cdot C'/M(\text{ZnSe})$, where $C[\text{at.}\%]$, $C[\text{cm}^{-3}]$ and C' are concentrations of the dopant in atomic percents, inverse cubic centimeters and fractions of one respectively, N_A is Avogadro constant, $\rho(\text{ZnSe})$ is the zinc selenide density in [g/cm^3], $M(\text{ZnSe})$ is the zinc selenide molar weight in [g/mol]. For example, to obtain ZnSe:Cr crystal with mass of 2.5 g and concentration of the dopant 0.03 at.% (0.0003, $6.5 \cdot 10^{18}$ cm^{-3}) it is necessary to use 1.1322 g Se, 1.3676 g Zn, 0.0002 g Cr.

The purity of the substances used in the technological processes is: double sublimated in vacuum Zn with initial purity of $\sim$99.9%, Se $\sim$99.99%, metallic Cr $\sim$99.8%, metallic Ni $\sim$99.8%, metallic Mn $\sim$99.8%, metallic Yb $\sim$99%, metallic Gd $\sim$99.9%. Inferior purity of the dopants should not have significant influence on the crystal properties because their concentration in the crystals is very low.

Synthesis from the elements and CVT crystal growth were performed in high vacuum pumped ($<$0.1 Pa) silica ampoules. Iodine ($\sim$99 % purity) amount introduced in ampoules was taken as 5 mg/cm^3. During synthesis, ampoule with substances was placed for 2-3 days in zone of reverse gradient, i.e. temperature in the source zone was smaller than in the growth zone. Such position prevents substance transport and allows to synthesize zinc selenide. Synthesis was performed at temperatures of $\sim$1020 K. After the synthesis, the ampoule was placed in the growth position with direct gradient (temperature in the source zone is 10-15 K higher than in the growth zone), in which it was maintained during the whole crystal growth time (8-14 days depending on the crystal dimensions). After the growth, ampoule was rapidly cooled to the room tem-

perature, at the same time the sample-free end of the ampoule was cooled quicker to guarantee solidification of the transportation agent in it. Grown crystals were washed in boiling ethanol to remove iodine from their surfaces. For study of properties single-crystal blocks were cut out from bulk samples by wire-saw, and the surface damaged by cutting was mechanically polished. The growth face, used for the PL study was not polished neither mechanically nor chemically. Growth by CVT method with iodine as transportation agent leads to inevitable background doping with iodine, therefore all crystal obtained by this technique will further be marked as [I].

Doping by high-temperature annealing in Bi melt (Bi $\sim$99.99 %) was also performed in sealed and pumped silica ampoules. Before annealing, all the samples were cut out from the intrinsic high resistivity n-ZnSe crystal grown from melt (by the Bridgman method) and mechanically polished for giving them a necessary shape. Prior to annealing, crystals' surface was cleaned by etching in solution of bromide in methanol (Br_2 + CH_3OH) and after that boiled in sodium hydroxide and deionized water. Annealing was performed for 120 h at 1160 K temperature. The ratio between the sample volume and melt volume was maintained 1:7, respectively, in every annealing process. The doping level was controlled by dopant (X) concentration in melt ((100 - C) at.% Bi + C at. % X). After annealing, the ampoules were turned in a way, which provides transfer of the melt to the sample-free end of ampoule, and then the samples were rapidly cooled to room temperature. Crystals were treated in a concentrated solution of iron chloride (III) to eliminate the rest of the melt after solidification, and next the samples were boiled in sodium hydroxide and deionized water. It should be mentioned that the high-temperature annealing of zinc selenide crystals in bismuth melt leads to their partial dissolution. Because of this, prior to study of samples' properties, all the crystals were newly mechanically polished and chemically etched in bromide in methanol solution. Selenium residuals, formed as a result of chemical etching, were eliminated from the samples' surfaces by the last boiling in concentrated solution of sodium hydroxide. Annealing in Bi melt leads to background doping with bismuth, therefore all crystal obtained by this technique will further be marked as [Bi].

The sample preparation of crystals doped by thermal annealing in Zn is the same as used for ZnSe [Bi] crystals. Annealing was performed for 100 h at 1200 K temperature. The ratio between the sample and melt volume was maintained 1:15, respectively, in every annealing process. The doping level was controlled by dopant (X) concentration in melt ((100 - C) at.% Zn + C at. % X). After the doping samples were quickly cooled to the room temperature, assuring transfer of the melt before its solidification

to the sample-free end of ampoule. Afterwards, samples were etched in HCl for the elimination of the soldered Zn remains from the surfaces, the last etching in the bromide and methanol solution and in sodium hydroxide was the same as for the ZnSe [Bi] series. Treatment in zinc melt leads to the strong deviation of stoichiometry in the crystals, decrease in zinc vacancy concentration (V_{Zn}) and increase of concentration of interstitial zinc (Zn_i), therefore all crystal obtained by this technique will further be marked as [Zn].

The difference in the doping temperature (annealing in the Bi melt was made at lower temperature) is caused by the higher zinc selenide solubility in liquid bismuth comparing to the liquid zinc. After the annealing in the Bi melt, samples lost some of their masses comparing to the initial samples, but annealing in the Zn melt does not have any significant influence on the mass or shape of the samples. It may be assumed that at lower temperatures, zinc selenide solubility in the liquid Bi is lower, however, lower annealing temperature will lead to lower dopant diffusion from melt into the sample. The maintenance of the doping level at the lower diffusion rates may be compensated by increasing the annealing duration: 120 h for annealing in Bi melt annealing, comparing to 100 h for annealing in Zn melt.

2.2 Characterization of photoluminescence and optical properties

Luminescent properties were studied on the measurement system designed for investigation of spectral properties within 0.2 - 4.0 μm wavelength region and 4 - 300 K temperature range. Functional scheme of the measurement system is presented in Fig. 3.

A pulse nitrogen laser (λ_{ex} = 337.1 nm $\pm$ 0.1 nm, pulse duration <3.5 ns, pulse energy 170 μJ, average power 3.4 mW) with a controlled pulse frequency (Fig. 3-1) was used for excitation of the emission in the visible spectral range. For suppression of the laser harmonics a narrow bandpass 337NB3 optical filter was used (transmission range 337.0 $\pm$ 0.6 nm) (Fig. 3-2). A green continuous wave (CW) laser Nd^{3+}:YAG (λ_{ex} = 532 nm, average power 330 mW) was used for excitation of the emission in the IR spectral range. CW laser beam was modulated with a mechanical SR540 chopper at 119 Hz frequency. The selection of modulation frequency f was conditioned by $1/f$ dependence of the registered noise, at the same time the upper frequency limit is determined by the lifetime of the excited state t_l ($1/2f \gg t_l$). Also, the modulation frequency should not be multiple to other frequencies used in the measurement system (e.g. power supply, data transmission, etc.), this allows to exclude registration of additional noise. Output of the Nd^{3+}:YAG was covered with a blue-green glass optical filter to cut the pumping

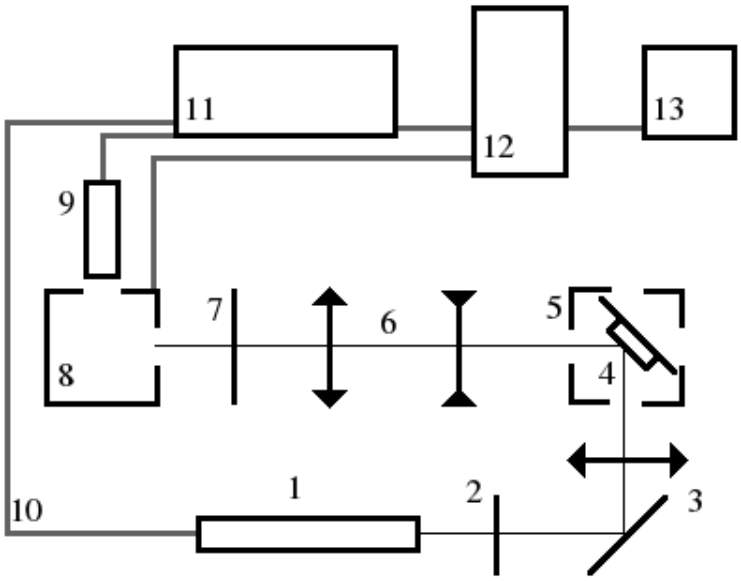

Figure 3: Functional scheme of the measurement system designed for investigation of PL properties: 1 - laser with the modulation system; 2 - optical filter; 3 - system of lenses and mirrors, 4 - sample; 5 - cryostat; 6 - optical condenser; 7 - optical filter; 8 - monochromator; 9 - photodetector; 10 - loopback connection for the phase sensitive detection; 11 - integrator and averager; 12 - computer interface; 13 - operating computer.

diode wavelength ($\sim$ 860 nm). An additional neutral optical filter with variable optical density NDL25S4 (Fig. 3-2) was used, when the dependence of the photoluminescence intensity versus excitation power was studied. A system of mirrors directed the laser beam on a thin lens (Fig. 3-3) that focused it on the sample (Fig. 3-4).

During the measurement the sample was mechanically attached to the cold finger of the continuously pumped open-flow helium cryostat Janis Research ST100 with quartz windows (Fig. 3-5). Temperature was detected by a silicon diode and controlled by the RVElektroniikka TS520 temperature controller. PL emission was focused by an optical condenser (Fig. 3-6) to the Oriel MS257 monochromator (Fig. 3-8) input slit. To protect the diffraction gratings from the reflected laser beam, as well as to exclude apparition of the diffraction gratings' replica, the monocromator's input slit was covered with an optical filter (Fig. 3-7): a white glass neutral Corning 0.51 with the absorption edge of $\sim$ 380 nm for measurements in the visible spectral range (420 - 800 nm), or interference IR filters with the absorption edge of 800 nm (FEL800) and 1500 nm (FEL1500) for the near-IR (800 - 1500 nm) and mid-IR (1500 - 3000) spectral ranges, respectively.

The MS257 monochromator represents an opto-mechanical system controlled either manually or via data transmission interface (RS-232 or GPIB). Mechanical part is presented by a rotating disc with a mounted quadruple grating turret drive allowing selection of the proper grating for different spectral ranges. The disc is controlled by a build-in step engine via a gear-drive. The optical system consists of diffraction gratings, and two mirrors (one spherical and one toroidal) that determine the light way. Light flux through the input and output ports is controlled by the slits with opening within 0 - 2.2 mm range (precision of 0.1 mm).

Emission on the output of monochromator was registered either by photomultiplier tube (PMT) Hamamatsu 943-02 (sensibility range 160 - 930 nm, response time 3 ns) or PbS photoresistor Hamamatsu P394A (sensibility range 1.0 - 3.6 μm) (Fig. 3-9). When the photoresistor was used its output electrical signal was preamplified by Brookdeal Precision ac Amplifier (Type 452) and Brookdeal Lock-in-Amplifier (Type 401) before transmission to the SRS Gated Integrator and Boxcar Averager (Model SRS250) (Fig. 3-10). The output signal of PMT was directly sent to the averager.

Electrical signal after averaging was sent to the Computer Interface (Model SRS 245) equipped with 13-bit digital-to-analog converter with precision not less than 2.5 mV (Fig. 3-7). The same interface was used for sending control sequences to monochromator.

The transmission spectra were studied on the same measuring system after few reconfigurations. The studied sample was placed between the output slit of monochromator (Fig. 3-8) and the photodetector (Fig. 3-9). A halogen lamp with a stabilized power supply was used as a light source. The modulation, optical and registration systems remained unchanged.

2.3 Characterization of electrical and magnetic properties

Electrical measurements were carried out in constant electric and magnetic fields by electrometric method for the samples in the dark. Measurable electrical quantities were Hall voltage and voltage along the sample. Basing on the geometry of the samples and measurable values the Hall coefficient was calculated as follows

$$R_H = \frac{E_H}{J_x B_z} = \frac{U_H d}{I_x B_z}, \tag{7}$$

where U_H is the Hall voltage, d is width of the sample in directions perpendicular to both electric and magnetic fields, I_x is the current applied to the sample and B_z is magnetic induction. Other main electrical parameters were extracted from combination

of Eqs. (1), (2) and (7).

Magnetic properties were measured with the superconducting quantum interference device (SQUID) magnetometer Quantum Design (QD) MPMS XL. The basics of SQUID magnetometer may be found elsewhere (e.g. [78]). In this thesis, three types of measurement were used to study magnetization: zero-field-cooled (ZFC), field-cooled (FC) and field dependences. In ZFC measurement the sample was cooled to the lowest studied temperature in absence of the external magnetic field, after the field was turned on and the temperature dependence was measured while the temperature increased. FC measurements were made by switching the external magnetic field on at the highest studied temperature and then measuring the temperature dependence while the sample was cooled. Field dependences were measured for ZFC samples. At the room temperature the whole system was degaussed every time before performing next type of measurement.

3 Influence of d-element dopants on physical properties of ZnSe crystals

3.1 Emission properties

3.1.1 ZnSe:Cr

One of the most studied TM doped zinc chalcogenide is ZnSe:Cr. Spectroscopic properties of this material are: close to one quantum efficiency at room temperature, wide absorption band near 1.8 μm, which allows optical pumping of intra-shell transitions with various methods and absence of significant absorption on excited state in middle-IR spectral range [51, 57, 79] make it a valuable source of coherent emission in middle-IR spectral range.

PL spectra of ZnSe:Cr crystals in exciton region for all doping impurity concentrations are presented in Fig. 4. Emission spectrum of undoped ZnSe [I] crystal shows a relatively broad band of edge emission (full width at half maximum (FWHM) is 46.4 meV) with maximum localized at 444.4 nm at liquid helium temperature. Considering the large FWHM of the band, it may be assumed that it is not elementary, but the temperature dependence of its maximum position repeats with high accuracy the shape of free exciton maximum position temperature dependence, calculated by Varshni equation [18, 80]. This reveals its excitonic nature and allows to conclude that the band consists of free exciton emission overlapped with few bound-exciton emission lines.

Increase of the chromium concentration in ZnSe [I] samples up to 0.05 at.% leads to the decrease of the band intensity and shift of its maximum position to 453.0 nm (Fig. 4-a). At the same time, the shorter wavelength components, caused by radiative recombination of excitons bound to native defects and iodine, practically disappear. Further increase of the chromium concentration up to 0.10 at.% or higher in reactor during the growth process leads to more significant decrease of the edge band intensity and increase of its FWHM, which includes spectral range from $\sim$436 nm to $\sim$455 nm. It should be mentioned that the decrease of the emission intensity in the visible spectral range with the increase of the doping impurity concentration in the zinc selenide crystals is characteristic for all the doping elements from the iron group, including chromium [81]. In addition, it could be observed that chromium-bound excitons are dominant in the spectrum of the crystal with 0.05 at.% doping impurity.

Taking into account that excitons bound to acceptors are placed in longer wavelength region of the PL spectra, we may use the Hynes' rule [82–84], establishing re-

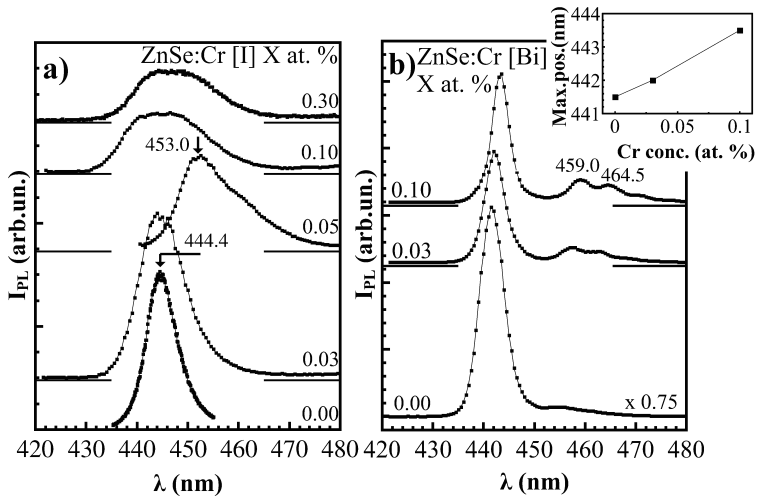

Figure 4: PL spectra of ZnSe:Cr [I] (a) and ZnSe:Cr [Bi] (b) crystals in exciton spectral range at T = 6.5 K. Inset: the dependence of the ZnSe:Cr [Bi] edge band maximum position on Cr concentration [**P1**].

lation between the acceptor level energy position (E_A) and exciton bound energy (E_B) $E_A = 10E_B$ to determine position of the energy level, responsible for formation of the long wavelength component of the edge band: E_A = 10 · (2.8015 eV – (1.239 eV · nm) / (453.0 nm)) = 0.66 eV. This value corresponds to position of the unexcited state of Cr^{2+} ion above the valence band of zinc selenide [85], if band gap is considered to be 2.820 eV at T = 4.2 K [18]. Also, it should be mentioned that the presence of excitons bound to chromium acceptor levels is in good agreement with known excitation mechanisms of chromium intra-shell emission in zinc selenide. Doubly charged chromium ions are considered to be acceptors in non-equilibrium state [51, 86].

Also, it is worth to mention that presence of excitons bound to chromium ions can not be observed in the PL spectra in form of individual bands or some particularities of the spectra. For example, chromium doping from the Bi melt (Fig. 4-b) does not lead to appearance of the features in ∼450 nm region of the PL spectra even in case of significant chromium concentration in the doping melt. However, increase of the chromium bound exciton contribution to the edge band emission may be observed from shift of the band to the long wavelength region of the spectra with chromium concentration increasing in the melt (Fig. 4(b), inset). Another detail characteristic for the increase of chromium impurity concentration in ZnSe:Cr [Bi] crystals is the increase of the PL band intensity with maximum close to 459.0 nm with its phonon replicas distanced 32

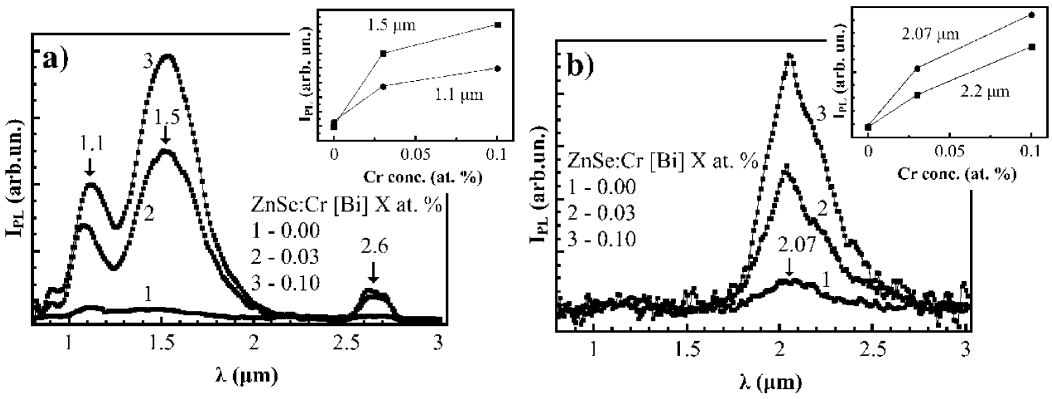

Figure 5: PL spectra of ZnSe:Cr [Bi] crystals in IR spectral range at T=6.5K (a) and T=300K (b). Inset: dependence of the emission intensity in the bands maximum on doping impurity concentration [**P1**].

meV from the main maximum, which corresponds to longitudinal optical (LO) phonon energy in zinc selenide. Position of this band maximum, as well as its shape with a few phonon replicas precisely corresponds to R_0 band, caused by emission transitions between donor complexes [Li_{Zn},V_{Se}] and acceptors Li_{Zn} [87]. Taking into account the possibility of non-radiative recombination of TM^{2+} bound excitons [86] as well as possibility of resonant energy transfer between chromium states and donor-acceptor pair [88], may be assumed that increase of the R_0 band intensity is caused by non-radiative transitions of a hole and an electron, forming an exciton bound to chromium impurity, to a donor and an acceptor, forming an appropriate DAP. This assumption is confirmed by closeness of recombination energy of DAP emission, resulting in R_0 band, and chromium bound exciton recombination energy, determined from PL spectra of ZnSe:Cr [I]. Presence of a small Stokes shift does not contradict the assumption. In this case the increase of the R_0 band intensity should be considered a result of the chromium doping. Also, the obtained result allows us to assume that the absence of the emission caused by radiative recombination of excitons bound to Cr^{2+} ions in ZnSe:Cr PL spectra may be caused by presence of a number of structural or impurity defects in the crystals.

The near-IR PL band located at ~ 0.95 μm in spectra of Cr-doped ZnSe crystals is usually attributed to $^3T_1 \rightarrow {}^5T_2$ intrashell transitions within Cr^{2+} ion [89]. In PL spectra of ZnSe:Cr [Bi] crystals this band is shifted to the long wavelength region of the spectra and its maximum is located near 1.1 μm (Fig. 5). This shift is probably caused by the partial overlapping of the band in near-IR spectral range with the PL band located close

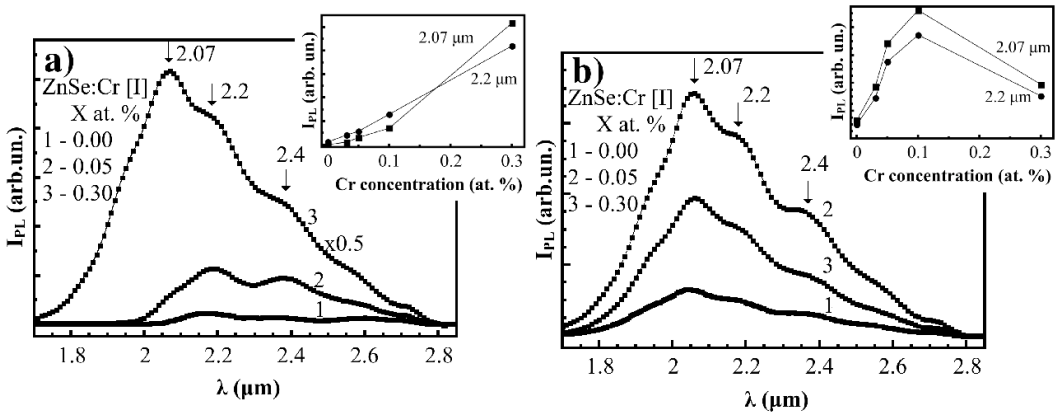

Figure 6: PL spectra of ZnSe:Cr [I] crystals in IR spectral range at T=6.5K (a) and T=300K (b). Inset: dependence of the emission intensity in the bands maximum on doping impurity concentration [**P1**].

to 1.5 μm, observed only in PL spectra of ZnSe:Cr [Bi] crystals. Taking into account the ability of Bi impurity to form point defects such as Bi_{Se} and Bi_i, as well as complexes with native impurities [90], it can be assumed that the band with 1.5 μm maximum is caused by incorporation of the bismuth atoms from melt. However, a strong dependence of emission intensity of the both bands located at 1.1 μm and 1.5 μm on the chromium concentration suggests that both bismuth and chromium impurities participate in the formation of the band.

In mid-IR spectral range a wide structural PL band with a few maxima may be observed (Fig. 6). The band's FWHM as well as the ratio of its primary and secondary maxima strongly depend on the crystal's doping method and temperature. At liquid helium temperatures and low concentrations of the chromium impurity, the main maximum is localized at 2.2 μm (Fig. 6-a). Increase of the chromium concentration leads to increase of 2.07 μm maximum even at low temperatures (Fig. 6-a, inset). At room temperature, the main peak is close to 2.07 μm in spectra of all studied ZnSe:Cr crystals (Fig. 6-b), which is in good agreement with data of more efficient emission of chromium ions in mid-IR spectral range when the temperature is increased [44]. The large FWHM of the discussed band, presence of few maxima in its shape, as well as change in the maxima ratio depending on the chromium concentration or doping method at low temperatures (Fig. 6-a, inset), allows us to conclude that 2.07 μm band is complex, consisting of a number of elementary bands. This assumption does not contradict

with the literature on intrashell emission of the chromium ions in IR spectral range, but may explain differences in experimental data presented in literature and enumerated in the section 1.5. Even more, secondary maxima repeat with sufficient accuracy position of the mid-IR band given in other papers [41–45].

In case the band with the main maximum at room temperature located at $\sim$2.07 μm is complex, we may try to associate its components with radiative transitions. The component located at 2.07 μm is most probably caused by intrashell transitions $^5E \rightarrow {}^5T_2$ within the Cr^{2+} ions. This is confirmed by its intensity dependence on chromium concentration (Fig. 6-a, inset); intensity increase with temperature, which may be evidence of higher emission efficiency at room temperature [44]; as well as the energy position of the emission being closest to theoretically calculated distance between ^5E and $^5T_2$ levels (2.04 μm) of Cr^{2+} ion [91]. Energy position of 2.2 μm component corresponds to the energy position of [V_{Zn}, Al_{Zn}] complexes within the ZnSe bandgap [3], but 2.4 μm component may be caused by associative defects of shallow donor impurity (for example, iodine) and zinc vacancies [3]. Particularly, in Ref. [92] it is communicated that presence of emission in mid-IR spectral region is characteristic for ZnSe crystals grown by CVT method with iodine as transportation agent. It should be mentioned that assumptions about the defect-impurity composition of the crystals made during analysis of IR PL spectra are in the good agreement with assumptions made in description of the visible PL spectra.

3.1.2 ZnSe:Ni

Influence of nickel impurity concentration on PL spectra of ZnSe:Ni in visible spectral range is shown in Fig. 7-a. At 6.5 K the PL spectra of the crystals mainly consist of an edge band and two wide PL bands localised in long-wavelength region at 537 nm (2.307 eV) and 612 nm (2.025 eV). Taking into account the large FWHM of 26 meV for the edge band and its shift towards long wavelengths in comparison to the free exciton (FE) line, this band may be considered to be a superposition of few bands caused by recombination of excitons bound to uncontrolled impurities and native defects, e.g. iodine, zinc vacancies or aluminum.

Excitation light power dependence of the edge PL intensity is presented in the inset of Fig. 7. It is well established that the PL intensity I increases with the excitation power P as $I \sim P^{\alpha}$ [93]. According to the previous studies, which are commonly accepted and independently confirmed for different material systems, the power factor α falls into one of the following ranges if the excitation energy is higher than the bandgap energy

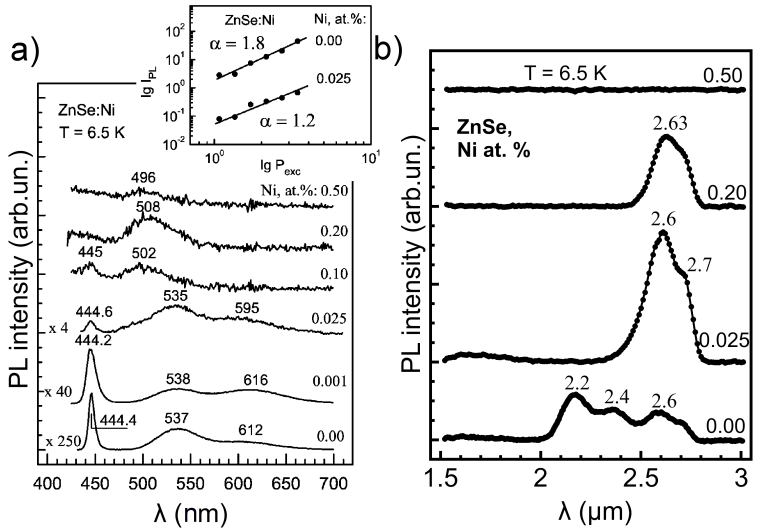

Figure 7: Influence of nickel impurity concentration on edge and visible (a) and IR (b) PL spectra of ZnSe:Ni crystals, measured at T = 6.5 K. Inset: the dependence of the edge band PL intensity versus the power of excitation light [**P2**].

as in our measurements. Power factor is in the range $1 < \alpha < 2$ for the bound-exciton emission, and in the range $0 < \alpha < 1$ for the free-to-bound radiative recombination, such as free hole and neutral donor recombination (h, D), free electron and neutral acceptor recombination (e, A), or donor-acceptor pair recombination (D, A) [94, 95]. In our case, $1 < \alpha < 2$, that confirms the excitonic nature of the edge PL band.

Broad and less intensive PL bands with maxima at 537 nm (2.307 eV) and 612 nm (2.025 eV) were observed earlier in PL spectra of ZnSe:Fe [**P8**], ZnSe:Mn [**P9**] and ZnSe:Cr [**P3**] crystals and were attributed to native defects. The band localised in this region was observed in PL spectra of the both undoped and halogen-doped ZnSe crystals and was regarded as a self-activated (SA) emission band [96]. The authors of [97] attribute this SA-band to DAP recombination within the (V_{Zn}-Cl_{Se}) complex centers. Taking into account that the crystals studied here were grown by iodine transport method, it is assumed that iodine atoms incorporate into the selenium sublattice during the growth process and form shallow hydrogen-like donors with the activation energy of 28-33 meV [98]. A part of the iodine ions may form (V_{Zn}-I_{Se}) complexes with native defects, responsible for the observed SA-emission in the undoped sample. The band with maximum at 612 nm is caused by DAP-recombination within the centers formed by V_{Zn} native defects and uncontrolled Al_{Zn} shallow donors [99].

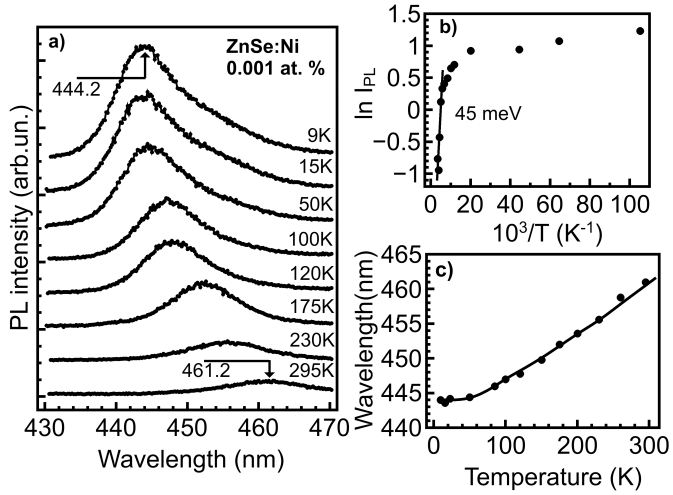

Figure 8: The temperature evolution (a), emission intensity versus inverse temperature (b) and spectral position versus temperature (c) of the edge band in the PL spectra of ZnSe:0.001 at.% Ni crystal [**P2**].

Light nickel doping (0.001 at.%) of ZnSe crystals changes the structure of the PL spectrum (Fig. 7-a) slightly: the intensity of the PL bands decreases more than 6 times, the edge band slightly shifts towards short wavelengths (444.2 nm) and the long-wavelength PL bands slightly shift to 538 and 616 nm, respectively. It is known that d-element dopants are the quenchers of visible PL in ZnSe. Incorporation of nickel ions into zinc sublattice of ZnSe leads to a decrease of V_{Zn} native defects concentration. As a result, the formation of (V_{Zn}-D) emission centers becomes less probable. This may explain the concentration quenching of the SA-bands. The increase of nickel concentration to 0.025 at.% leads to a further decrease of the edge PL band intensity and its shift towards long-wavelengths. Intensities of the long-wavelength visible PL bands also decrease. At nickel concentrations of 0.20 and 0.50 at.%, the edge and long-wavelength PL bands are practically quenched and only a weak PL band with maximum at 496 nm may be observed (Fig. 7-a). A similar band with maximum at 488 nm, observed in PL spectra of ZnSe crystals grown in the presence of H_2 vapors, was attributed to DAP-recombination of associative emission centers based on V_{Zn} native defect and oxygen impurity [100].

Temperature influence on ZnSe:Ni (0.001 at.% Ni) edge PL spectra is shown in Fig. 8-a. The temperature increase leads to a decrease of the edge band intensity, an increase of its FWHM and its shift towards long wavelengths. The process of PL temperature

quenching may be described in general case by equation [93, 101]

$$I(T) = \frac{I_0}{1 + A \exp\left(\frac{-E_A}{k_B T}\right)}, \tag{8}$$

where I_0 is the maximum intensity of the PL band in the absence of temperature quenching, E_A is the activation energy of PL temperature quenching, k_B is the Boltzmann constant and A is a proportionality constant. The PL band intensity versus inverse temperature and its spectral position versus temperature are presented in Figs. 8-b and 8-c, respectively. The edge band emission starts to quench at temperatures above 50 K with the quenching energy of ∼45 meV (Fig. 8-a). The hole binding energy to Ni impurity in ZnSe:Ni crystals is estimated to be 37 meV [102], and the binding energy of the exciton to the same impurity should be larger [2], corresponding to our experimental value of the activation energy of thermal quenching. Considering that Ni-bound excitons have a major contribution to the edge band, we may use the Haynes' rule [82, 83] to estimate the energy of optical transition responsible for this PL band: E = 10 · 45 meV = 450 meV. According to Ref. [103], the $^3T_2$ level of $Ni^{2+}\{d^8\}$ ion is localized 540 meV above the ZnSe valence band top. It gives reason to conclude that the edge PL band in ZnSe:Ni crystals is caused by a superposition of at least two lines: V_{Zn} acceptor bound exciton (ABE) (I_1^d) and $Ni^{2+}\{d^8\}$-ABE. The obtained value of 450 meV for the energy of optical transition in the exciton emission range is less than the localization energy of $^3T_2$ level for $Ni^{2+}\{d^8\}$ ion, given in Ref. [103]. This inconsistency between the value obtained from the presented results and values reported previously may be caused by an error in determination of the activation energy of the edge band temperature quenching. The contribution of V_{Zn}-ABE (I_1^d-line) to the edge band may slightly lower the temperature quenching activation energy since the localization energy of V_{Zn} acceptor is 220 meV [104]. With increasing temperature, maximum of the edge PL band shifts monotonically towards long wavelengths (Fig. 8-c), which corresponds to the shift of free exciton peak position according to the Varshni equation. This fact is an additional confirmation of excitonic nature of the edge PL band in the PL spectra of ZnSe:Ni samples.

Low-temperature (6.5 K) mid-IR PL spectra of ZnSe crystals doped with various Ni concentrations are presented in Fig. 7-b. Large emission bands with maxima at 2.2, 2.4 and 2.6 μm are observed in the PL spectrum of undoped ZnSe crystal. A light nickel doping (0.025 at.%) of the samples leads to appearance of only one emission band in IR PL spectrum with maximum at 2.6 μm and a peculiarity on the long-wavelength "wing" at 2.7 μm that indicates a complex structure of the band. The increase of Ni

concentration to 0.20 at.% results in a broadening of the IR PL band, a slight shift of its maximum towards long wavelengths (2.63 μm) and a decrease of the band intensity. A further increase of the doping impurity concentration up to 0.50 at.% leads to quenching of the IR emission in the studied spectral range.

The IR PL band with maximum near 2.16 μm was earlier observed in PL spectra of ZnSe:Fe [**P8**] and ZnSe:Cr [**P3**] crystals. It was attributed to chromium uncontrolled impurity or complexes, which include V_{Zn} native defects [**P1**]. An IR PL band with maximum at 2.4 μm was observed for the crystals grown by iodine-transport technique and was attributed to iodine-based complex emission centers [92]. The studied crystals are grown by the same method, and therefore it may be considered that the observed IR PL band at 2.4 μm in 6.5 K spectrum for undoped crystal is caused by complex emission centers based on iodine impurity and zinc vacancy. Nickel doping of the studied crystals quenches this PL band intensity. Nickel incorporates into the zinc sublattice and decreases the concentration of V_{Zn} native defects, therefore, the formation of the complex emission centers based on iodine impurity and zinc vacancy, becomes less probable. The band with maximum at 2.6 μm in IR PL spectra of undoped ZnSe crystals was attributed to uncontrolled impurities [92], e.g. nickel contamination of the zinc used for the crystal growth.

The increase of Ni concentration to 0.20 at.% decreases the band intensity, increases its FWHM and slightly shifts the maximum to 2.63 μm (Fig. 7-b). Thus, the maximum intensity of the nickel intrashell emission is obtained for Ni concentration of $\sim$0.025 at.%. This correlates well with the data obtained from the study of visible PL spectra, when at the same concentration, the shift of the edge band becomes more prominent. For nickel impurity concentrations above 0.50 at.%, IR emission is quenched due to concentration quenching as observed earlier [92, 105].

3.2 Magnetic properties

3.2.1 ZnSe:Cr

At sufficiently low temperatures and TM impurity concentrations, the magnetization of DMS may be expressed as the sum of contributions from magnetic centers and diamagnetic crystal host [106]. In Fig. 9, the field dependence of the magnetization in ZnSe:Cr [I] crystals is presented. The magnetization of the undoped crystal has a positive sign and the value is significantly larger than that of the chromium doped samples. This may be explained by paramagnetic contribution of [I_{Se},V_{Zn}] centers [3]. These com-

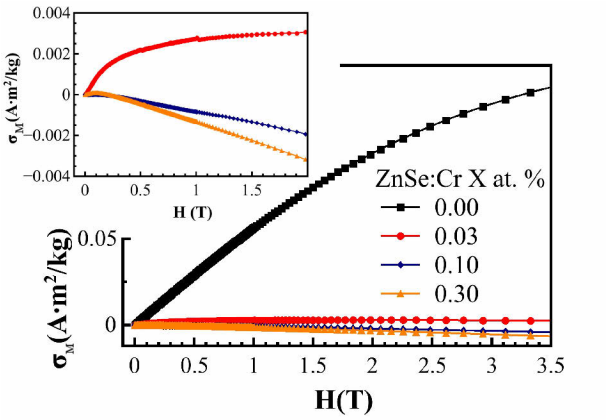

Figure 9: The field dependence of ZnSe:Ni crystals magnetization at T=5 K (inset is enlargement of 0.03 - 0.30 at. % Ni samples) [**P3**].

plexes could be formed during the CVT growth process because of the iodine used as the transport agent. However, the saturation, which starts to appear at fields higher than 3 T, may indicate some amount of the uncontrolled magnetic impurities, e.g. TM ions, which are typical background dopants for the zinc chalcogenide crystals [30]. Doping with chromium leads to significant decrease of the magnetization values and to inversion of the magnetization sign at concentrations of the doping impurity higher than 0.10 at.% Cr. The negative values of magnetization are most probably caused by diamagnetic contribution of the zinc selenide crystal lattice. This should be larger than the sum of paramagnetic contribution from [I_{Se},V_{Zn}] complexes and contribution from the chromium ions. Decrease of the paramagnetic contribution from iodine-based complexes may be caused by decrease of its concentration due to the Cr-doping. Chromium ions incorporate into the zinc sublattice nodes [81, 107], thus chromium doping significantly reduces number of zinc-vacancy nodes, which take part in the formation of [I_{Se},V_{Zn}] paramagnetic centers. At the same time, low chromium concentrations in the source materials (0.03 at.%) decrease the value of magnetic field at which the saturation begins (Fig. 9). This indicates some increase in the concentration of the ferromagnetic centers within the crystals.

The hysteresis loops were measured to prove that chromium doping of the zinc selenide crystals leads to increase of the concentration of ferromagnetic centers. The Fig. 10 confirms this for concentrations less than 0.05 at.% Cr. It may be observed that undoped crystal has no remanent magnetization ($M_R \sim 6 \cdot 10^{-9}$ A·m^{-1}, which is

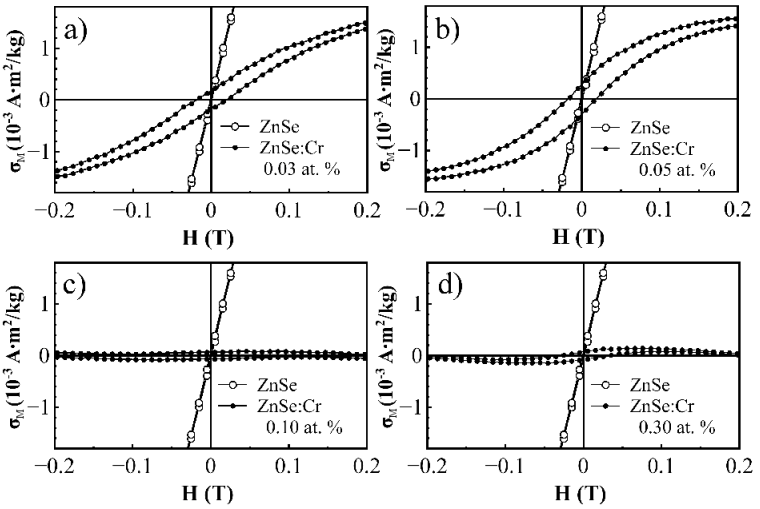

Figure 10: The hysteresis loops of ZnSe:Cr crystals with dopant concentration of 0.03 (a), 0.05 (b), 0.10 (c) and 0.30 (d) at.% Cr at T=5 K [**P3**].

near the measuring precision). Adding of small amounts of chromium impurity to the source material during the growth process results in appearance and enlargement of the remanence of the hysteresis loop ($\sigma_{\mathrm{R}} \sim 1.8 \cdot 10^{-4}$ A·m^2/kg in case of 0.03 at.% Cr and $\sigma_{\mathrm{R}} \sim 2.9 \cdot 10^{-4}$ A·m^2/kg for 0.05 at.% Cr). Also, as it was observed from the magnetization field dependences, chromium doping leads to the lowering of the magnetic field, at which saturation begins, to $\sim$0.2 T. Determination of the saturation magnetization, σ_S, can not be done precisely because of two additional contributions: paramagnetic from the [I_{Se},V_{Zn}] complexes, concentration of which is smaller when the chromium doping level is higher, and diamagnetic, which comes from the ZnSe crystal lattice and should be independent on the chromium doping. However, increase of the doping level from 0.03 at.% Cr to 0.05 at.% Cr leads to increase of the σ_{S} from $\sim 1.2 \cdot 10^{-3}$ A·m^2/kg to $\sim 1.5 \cdot 10^{-3}$ A·m^2/kg, eventually increase of the saturation magnetization should be higher, because the used experimental values do not take into account decrease of the paramagnetic contribution to the magnetization. Increase of the chromium concentration in the samples above 0.10 at.% leads to decrease of the remanent magnetization value to $\sim 6.5 \cdot 10^{-5}$ A·m^2/kg. This univocally indicates that ferromagnetic properties of ZnSe crystals, which appear because of the chromium doping, become weaker at concentrations of the doping impurity higher than 0.05 at.%.

The oscillating change in the magnetic properties of the ZnSe crystals (increase

and decrease of the remanent magnetization with increasing Cr impurity concentration) may be explained, for example, by the RKKY theory. Taking into account that p-type conductivity in bulk ZnSe samples is almost unreachable [81], we may consider only the carriers in the conduction band. In such a case, the effective coupling (J_{sd}) will be simply proportional to the RKKY-function, but its sign, which determine the type of magnetic interaction between the localised spins, will correspond to the sign of the RKKY-function. Considering that chromium impurity in the crystals is distributed uniformly, we may approximate the distances between the Cr ions for the concentrations 0.03, 0.05, 0.10, 0.30 at.% Cr as 6.6, 5.6, 4.4, 3.0 nm, respectively. These can be used to analyze the results with Eq.(5), using the k_F as a fitting parameter. The best fitting (RKKY-function is positive for 0.03 and 0.05 at.% Cr samples and negative for 0.10 and 0.30 at.%) was obtained for k_F=0.8 nm^{-1}, which corresponds to $n \sim 10^{19}$ cm^{-1}. For this electron concentration, electron gas in ZnSe crystal should be degenerated [108], but experimentally measured resistance does not confirm this since the resistance of the samples measured at room temperature is of the order of MΩ. The argument ξ of the RKKY-function is the product of the Fermi wavevector and the distance between the magnetic impurities. This means that smaller values of k_F, corresponding to the lower free electron concentrations, fits the experimental result if the distance between magnetic impurities is proportionally higher. Reasonable values of k_F for the measured resistance of the samples fit the results with 2-3 times larger distances between the chromium atoms.

It is well-known that TM in the II-VI materials may form homonuclear pair [58, 109], e.g. Cr^{2+}-Cr^{2+}. Formation of these pairs may explain larger distances between magnetic ions in the studied crystals, however, the presence of these centers excludes possibility of the direct application of the RKKY-interaction to explanation of the results. The concentration of TM-TM pairs or complexes most often follows statistical laws [58]. This means that concentration of these centers depends on the concentration of chromium impurity in the crystals, and assumption about random and uniform distribution of the doping impurity can not be applied to the whole concentration range. At the same time, the presence of Cr-Cr pairs may qualitatively explain the obtained results. At large distances between the chromium ions, Bethe-Slatter curve predicts the parallel orientation of the magnetic moments with a maximum of the J value at some certain distance between the impurities [110]. However, the Bethe-Slatter curve may be applied only in case of the direct interaction between the ions and is mostly determined by the balance between the Coulomb and kinetic energies. Direct interaction for the studied

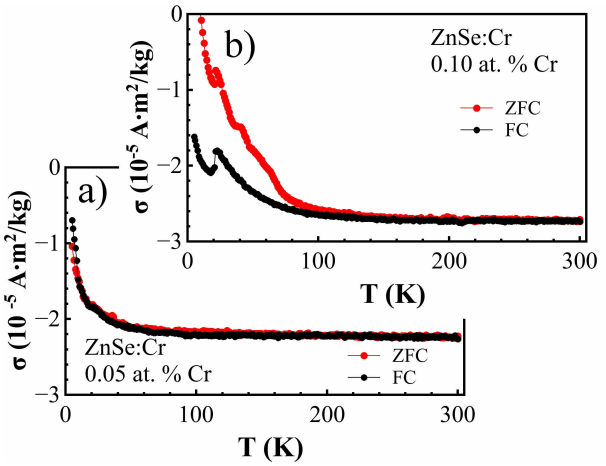

Figure 11: The magnetization temperature dependence of ZnSe:Cr 0.05 at. % (a) and ZnSe:Cr 0.10 at. % (b) crystals, open circles show field-cooled (FC) data and filled circles show zero-field-cooled (ZFC) data, B=10 mT [**P3**].

concentration of the chromium impurity is possible only by means of the tunneling of electrons between two neighbouring Cr ions. Regardless the large interatomic distances aproximated above, it is known that at low temperatures tunneling to the distant atom has higher probability than tunneling to the closer one [111]. Thus, direct interaction via tunneling of electrons may explain ferromagnetic behaviour of the ZnSe:Cr samples at concentrations of the doping impurity less than 0.05 at.%. At high chromium concentration, doping impurities start to form pairs, in which magnetic moments of the consisting ions are antiparallel. This may also be confirmed by the Bethe-Slatter curve, which predicts antiferromagnetic properties of two chromium ions situated at distances comparable with the radius of the incompletely filled shell [110]. Antiparallel orientation of the magnetic moments results in decrease of the σ_S as well as the area of the opening on the hysteresis curve, observed experimentally.

The assumption made about the formation of chromium homonuclear pairs at concentrations above 0.05 at.% Cr may be confirmed by the temperature dependence of magnetization (Fig. 11). The FC and ZFC temperature dependences of ZnSe:Cr 0.05 at.% crystal magnetization coincide, at the same time, temperature dependence of magnetization of ZnSe:Cr 0.10 at.% crystal shows a behaviour characteristic for spin-glasses. Spin-glass behaviour will mean the presence of both ferromagnetic (isolated Cr ions) and antiferromagnetic (Cr-Cr pairs) centers.

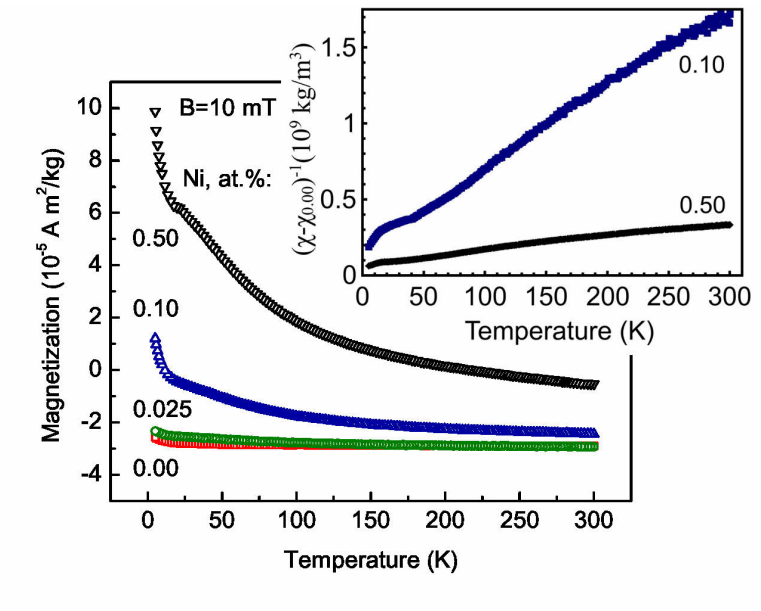

Figure 12: Temperature dependence of magnetization for ZnSe:Ni samples and inverse magnetic susceptibility (insert), B = 10 mT [**P2**].

3.2.2 ZnSe:Ni

The magnetic properties of the studied ZnSe samples with various Ni concentrations are presented in Fig. 12. FC and ZFC temperature dependences of the sample magnetization coincide, therefore, only one of them is shown.

Assuming that the distribution of the Ni ions in the host crystal follows the statistical law

$$p_i = C_i^4 x^i (1-x)^{4-i}, \tag{9}$$

where p_i means the number of unit cells containing i Ni ions, $C_i^n = n!/i!(n-i)!$ and i = 0, 1, 2, 3, 4, one can find that the majority of unit cells (about 97.82%) do not contain Ni ions and 2.16% of unit cells contains one Ni ion. The fraction of unit cells with 2 (pairs) or more (trimers and tetramers) nickel ions is about 0.02% and, therefore, their influence on the magnetic behavior of the studied crystals can be neglected.

However, the detailed analysis of the magnetic curves measured at various concentrations of Ni impurity demonstrates that they cannot be obtained from each other by simple scaling (compare the curves for 0.1 and 0.5 at.% Ni). The change in the impurity concentration leads to the change in the curvature of the χT curves. The intersection of

the extrapolated linear section of the curve with the temperature axis also changes from $\sim$ - 20 K in case of the 0.10 at.% sample to $\sim$ - 80 K for the 0.50 at.% concentration (Fig. 12, inset). Formation of the exchange coupled Ni pairs in the amount sufficient to affect slightly the magnetic behavior of the whole crystal may take place as it was reported in [**P3**] for ZnSe samples doped with Cr.

Another explanation of a slight difference of the χT curves shape can be based on the presence of few kinds of magnetic centers, contribution of which changes with increasing Ni concentration. For example, it is known that Ni ions occupy Zn sites, thus, Ni doping leads to decrease in zinc vacancy concentration. It is also known that paramagnetism of iodine-doped zinc selenide crystals arises from paramagnetic contribution of (V_{Zn} - I_{Se}) complexes [3], amount of which decreases with decreasing concentration of V_{Zn}. Decrease in the concentration of iodine- and zinc vacancy-based complexes, resulting from the nickel doping, leads to the formation of other types of iodine-based defects, e.g. (I-Zn-I) or (I-I), which are diamagnetic [112]. Presence of the different types of magnetic centers and their combined influence on the crystals magnetic properties may also explain the complex shape of the magnetization temperature dependence (Fig. 12).

3.3 Comparative analysis of TM doped ZnSe crystals

The main bands observed in PL spectra of the studied samples are summarized in Table 3. Comparative analysis of PL and magnetic properties of ZnSe:Fe [**P8**], ZnSe:Mn [**P9**], ZnSe:Cr [**P3**] and ZnSe:Ni [**P2**] crystals allows to conclude that only double charged TM ions (e.g. Cr^{2+} or Ni^{2+}) actively participate in formation of emission bands in visible and IR spectral ranges. Presence of TM^{2+} ions in the crystals leads to formation of TM-ABE, however, influence of these excitons on the emission properties strongly depends on the background impurities and native defects, thus, it depends on the doping method. In the mid-IR spectral range TM^{2+} ions give rise to broad intrashell emission bands, position of these bands depends on the type of ion and of possible resonance energy transfer between the ion and other emission centers. Presence of TM charge states other than TM^{2+} can not be excluded, even more, it may be assumed that TM^{+} ions are involved in photoexcitation processes. However, the present study allows to think that TM charge states other than 2+ will act as non-radiative recombination centers.

Concentration quenching of the TM activated emission was observed for all studied samples. For a long time, TM ion "agregates" are considered one of the most probable mechanisms for the concentration quenching, but its origin was unclear [43]. Compar-

Table 3: Main PL bands in emission spectra of ZnSe crystals.

Position at T $\sim$ 5 K	**Description**	**Ref**
439.5 nm	CB to VB transitions	[46]
441.5 nm	Recombination of free excitons	[46]
444 - 446 nm	Complex edge band (bound excitons)	[**P3**], [**P2**]
453.0 nm	Cr^{2+} bound excitons	[**P1**]
458.9 nm	R_0-band: [Li_{Zn}, V_{Se}]$\rightarrow$$Li_{Zn}$ transitions	[87]
460.1 nm	Q_0-band: $Al_{Zn} \rightarrow Li_{Zn}$ transitions	[87]
$\sim$ 488 nm	recombination within the centers based on V_{Zn} and oxygen impurity	[100]
$\sim$ 540 nm	self-activated emission: recombination within the (V_{Zn}-Cl_{Se}) complex centers	[97]
$\sim$ 0.95 μm	$^3T_1 \rightarrow {}^5T_2$ intrashell transitions within Cr^{2+} ion	[89]
$\sim$ 1.5 μm	probably Bi-based centers	
2.07 μm	$^5E \rightarrow {}^5T_2$ intrashell transitions within the Cr^{2+} ions	[44, 51]
$\sim$ 2.2 μm	[V_{Zn}, Al_{Zn}] to VB	[3]
$\sim$ 2.4 μm	[I_{Se}, V_{Zn}] to VB	[3]
$\sim$ 2.6 μm	$^3T_2(^3F) \rightarrow {}^3T_1(^3F)$ intrashell transition within Ni^{2+} ion	[45, 113]

ative study of both magnetic and luminescent properties allows us to conclude that in some cases (e.g. Cr and Mn) formation of homonuclear pairs is confirmed by the magnetic interaction between the ions, which has further influence on the emission properties. At the same time, the present study allows to assume that simultaneous usage of both optical and magnetic properties of ZnSe:TM crystals in practical applications may be difficult, because the highest emission efficiency from the crystal may be obtained at low TM^{2+} concentration, when magnetic properties exhibited by the TM ions are weak and comparable by the value with crystal host or uncontrolled defects magnetism. The effects, caused by high concentration of the TM doping impurity, may be interesting for some magnetic applications, however, they lead to formation of different magnetic centers on the TM basis, which have negative influence on the emission properties of the crystals.

4 Influence of f-element dopants on physical properties of ZnSe crystals

4.1 Emission properties

Photoluminescence spectra of ZnSe:Yb [I] crystals in the visible spectral range for a few doping impurity concentrations are presented in Fig. 13-a. The edge emission band is relatively broad. Considering the large FWHM of the band, it may be assumed that it is not elementary, but the temperature dependence of its maximum position repeats with high accuracy the shape of free excitons temperature dependence of the maximum position, calculated by Varshni equation [18, 80]. This reveals its excitonic nature and allows to conclude that the band consists of few overlapped emission bands caused by radiative recombination of excitons bound to different impurity centers. Increase of the Yb impurity concentration in the source material leads to increase of the edge bands FWHM (e.g. 47.8 meV for ZnSe:Yb [I] 0.20 at. % and 58.7 meV for ZnSe:Yb [I] 2.00 at. %), which indicates an appearance of some additional components in the edge band structure. The same conclusion may be stated based on the weak change of the edge band shape, which extends to the smaller wavelengths at Yb concentrations below 0.20 at. % and to smaller photon energies at Yb concentrations above 0.30 at. %. However, this extensions of the band are unsignificant and do not change the position of the edge band maximum. All these facts allow us to conclude that the influence of Yb doping on the edge emission of ZnSe crystals grown by CVT method and doped during the growth is weaker than the influence of the background defects introduced in the crystals by the growth method.

The same conclusion may be obtained from the dependence of the temperature quenching activation energy on the Yb concentration. Activation energy calculated from Eq. (8) is equal to 24$\pm$2 meV for the all studied concentration ranges of Yb impurity in ZnSe crystals. This temperature quenching activation energy with high accuracy corresponds to energy position of halogen impurities within zinc selenide bandgap [98, 114]. This indicates that there are excitons bound to iodine and chlorine impurities in the edge band spectra. The presence of halogens in the samples grown by CVT method may be explained by iodine usage as a transport agent, which has stronger influence on the PL spectra than the Yb doping impurity. Broad and structured bands of SA luminescence were discussed earlier (see section 3.1.2).

PL spectra of ZnSe:Yb [Bi] crystals in the visible spectral range consist only of the bands in the exciton region (Fig. 14-a). The edge band with the maximum at 446.6 nm

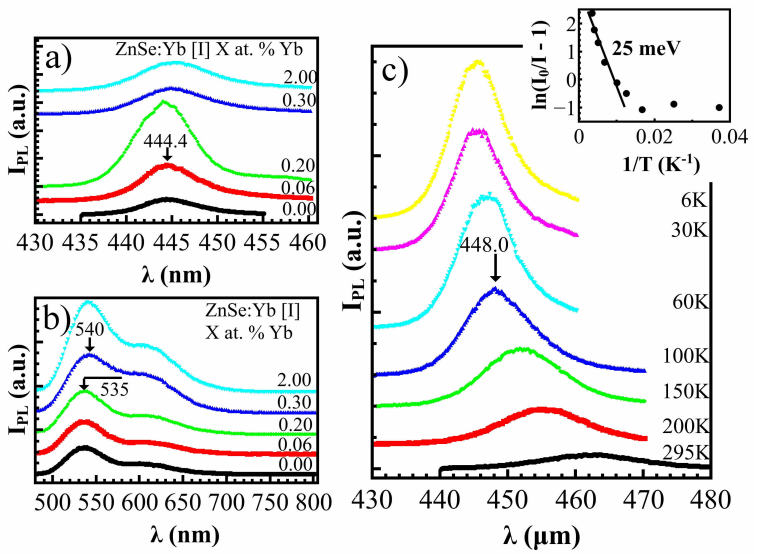

Figure 13: Visible PL spectra of ZnSe:Yb [I] crystals in excitonic (a) and long-wavelength (b) regions at T = 6.5 K. The temperature evolution of the ZnSe:Yb [I] 2.00 at. % PL band in the excitonic region (c). Inset: determination of the edge band thermal quenching activation energy [**P4**].

is significantly shifted to the longer wavelengths comparing to the free exciton emission. Position of the band does not change with the change of Yb impurity concentration in the doping melt, and the Yb doping results only in change of the edge band intensity. This behavior of the edge emission of the ZnSe:Yb [Bi] crystals is very similar to the previously observed for ZnSe:Yb [I] and allows us to assume that the Bi impurity, as well as iodine, has stronger influence on the PL properties of the zinc selenide crystals than Yb ions. This conclusion is also confirmed by the temperature quenching activation energy of the edge band (Fig.14-c). The energy calculated from the Eq. (8) is equal to 33±2 meV for the whole studied ytterbium concentration range. This value corresponds to the deep donor activation energy in the Bi-doped ZnSe crystals [115]. The obtained value of the activation energy leads to the conclusion that annealing in Bi melt performed in this study leads to formation of donor-like Bi complexes (e.g. Bi_{Se}-Zn-V_{Se} or Bi_{Se}-Bi_{Zn} [90, 115]). The similarity of iodine and bismuth sites explains the similarity of the observed emission properties of ZnSe:Yb [I] and ZnSe:Yb [Bi] crystals.

The structured band with the main maximum localised at 460.1 nm, with its phonon replicas distanced 32 meV from the main maximum, which corresponds to LO-phonon

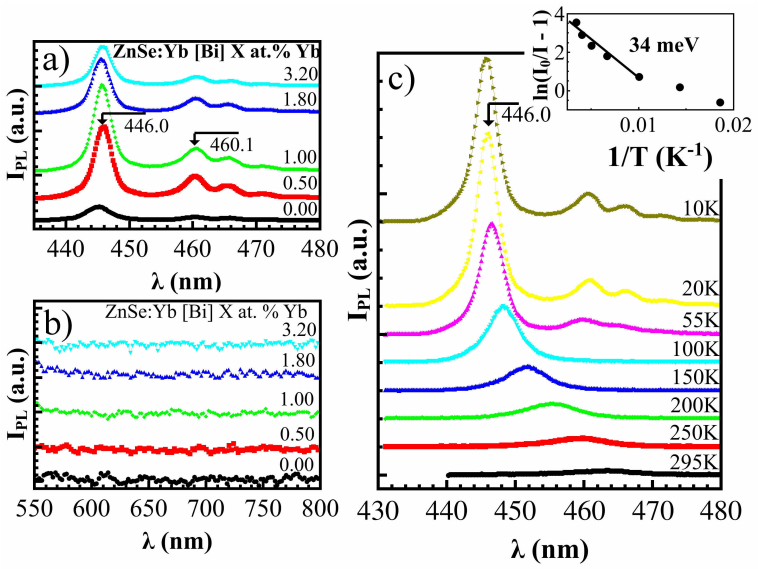

Figure 14: Visible PL spectra of ZnSe:Yb [Bi] crystals in excitonic (a) and long-wavelength (b) regions at T = 6.5 K. The temperature evolution of the ZnSe:Yb [Bi] 6.00 at. % PL band in the excitonic region (c). Inset: determination of the edge band thermal quenching activation energy [**P4**].

energy in zinc selenide, may be associated with the radiative DAP recombination (Fig. 14 (a)). Position of this DAP-band in the spectra of ZnSe:Yb [Bi] crystals, as well as its shape with few phonon replicas, precisely corresponds to Q_0 band [87].

PL spectra of the ZnSe:Yb [Zn] in the visible spectral range consist of three bands (Fig. 15): a band in exciton region, emission caused by DAP-recombination and a long-wavelength visible band, localized near 545 nm in the undoped crystal. In contrast to iodine and bismuth co-doped crystals, ytterbium doping has a significant influence on all parameters of the edge band emission in the spectra of ZnSe:Yb [Zn] crystals: the maximum position, FWHM and temperature quenching activation energy change. The transformation of the edge emission with increase of the Yb concentration in the doping melt reveals significant changes in the crystal's defect-impurity composition. Particular interest should be paid to the change of the temperature quenching activation energy of the band (Fig. 16). In the case of ZnSe:Yb[I] and ZnSe:Yb [Bi] crystals, the value of activation energy corresponds to the ionization of the iodine and bismuth impurity respectively and does not depend on the Yb impurity concentration. In the case of ZnSe:Yb [Zn] crystals, ytterbium doping leads to disappearance of the 63 meV

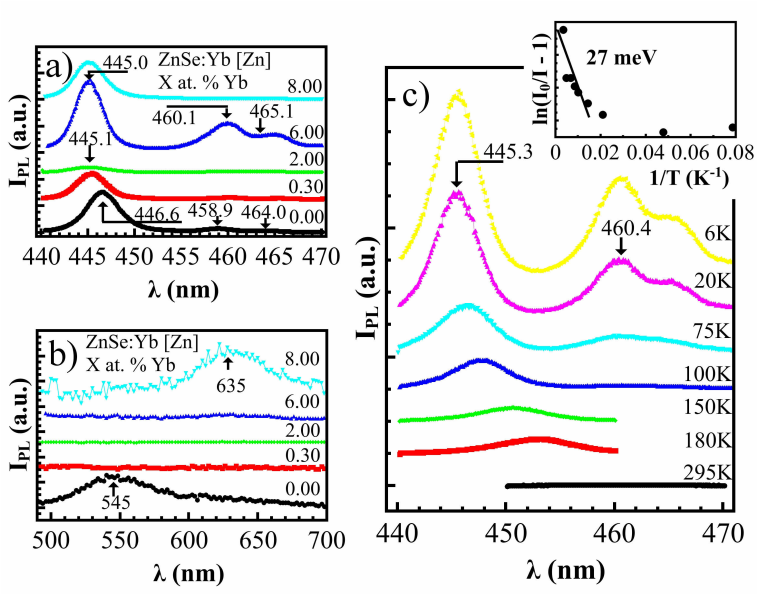

Figure 15: Visible PL spectra of ZnSe:Yb [Zn] crystals in excitonic (a) and long-wavelength (b) regions at T = 6.5 K. The temperature evolution of the ZnSe:Yb [Zn] 1.00 at. % PL band in the excitonic region (c). Inset: determination of the edge band thermal quenching activation energy [**P4**].

activation, which corresponds to ionization of [Li_{Zn}, V_{Se}] or [Na_{Zn}, V_{Se}] complexes [87]. At the same time, the maximum of the DAP-band shifts from 458.9 nm (R_0-band, caused by [Li_{Zn}, V_{Se}]→Li_{Zn} transitions) to 460.1 nm (Q_0-band, caused by $Al_{Zn} \rightarrow Li_{Zn}$ transitions) with increase of Yb concentration in the doping melt from. In both of these, the activation energies change and the shift of the DAP-band suggest destruction of the selenium vacancy based complexes [**P5**].

Emission spectra of the ZnSe:Yb [I] crystals in the IR spectral range are presented in Fig. 17. The two bands with maxima at $\sim$ 0.95 μm and $\sim$ 2 μm dominate the spectra. These two bands are usually referred as intracentral transitions within the chromium ions in ZnSe crystals [51]. Chromium, as well as iron, copper and other transition metal impurities, are typical contaminants of II-VI semiconductor compounds [30]. In mid-IR spectral range (Fig. 17-b), the increase of the ytterbium concentration in the crystals leads to the shift of the main maximum of the structured band to the smaller wavelengths. The same situation was observed in the case of ZnSe:Cr [I] crystals, when increase of chromium concentration leads to shift of the band's maximum and increase

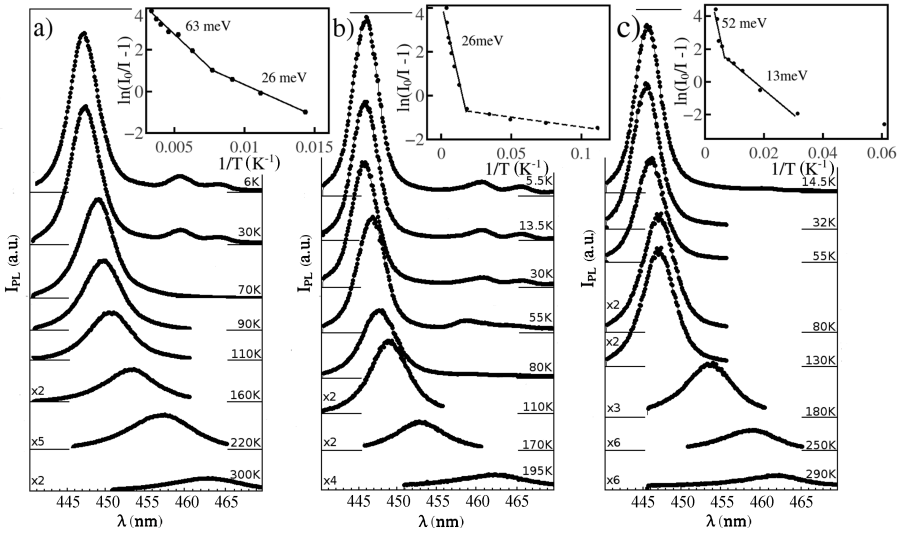

Figure 16: Temperature evolution of PL bands in exciton spectral region for ZnSe (a), ZnSe:Yb 0.03 at.% (b) and ZnSe:Yb 8 at.% (c) crystals. Inset: determination of thermal quenching activation energy [**P5**].

of the band's intensity [**P1**]. Thus, it may be considered that ytterbium, with concentrations below 0.30 at. %, acts as sensitizer for the chromium emission in the mid-IR spectral range. Taking into account that the band with the maximum at ~ 2 μm is complex and includes [I_{Se}, V_{Zn}] complexes. This emission is generated by the resonance energy transfer from the chromium ions (see section 3.1.1). It may be assumed that similarity of the Yb and Cr doping is caused by destruction of iodine-based complexes with increase of ytterbium concentration. In the analysis of the visible PL spectra, it was shown that efficiency of ZnSe activation with ytterbium strongly depends on concentration of selenium vacancies or selenium substituting centers, and thus it may be considered that concentration of I_{Se} defects and complexes on their basis will decrease with increasing of ytterbium concentration in the crystals. Decrease of [I_{Se}, V_{Zn}] complexes' concentration will eliminate energy transfer channel from the Cr^{2+} ions, and thus the intensity of competitive intrashell emission should increase. The consistent shift of the mid-IR band maximum also confirms this assumption, because the shift indicates the increase of the chromium ions emission contribution to the band comparative to emission from the [I_{Se}, V_{Zn}] complexes, for which emission is located at larger wavelengths. The decrease of the mid-IR band intensity at large Yb concentration (Fig. 17-b) may be a sign of Yb-complexes' formation, which lead to "purification" of the

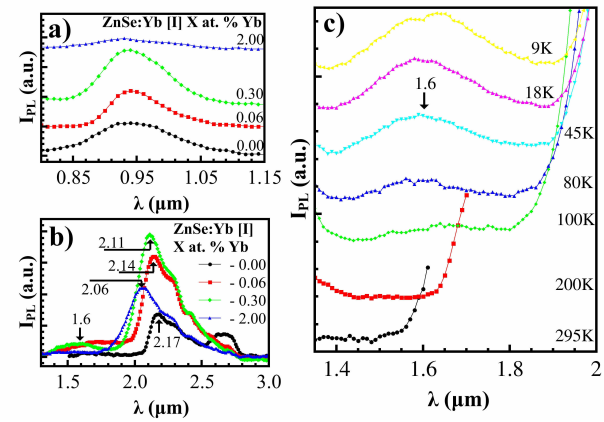

Figure 17: PL spectra of ZnSe:Yb [I] crystals in near-IR (a) and mid-IR (b) regions at T=6.5 K. The temperature evolution of the ZnSe:Yb [I] 0.10 at. % PL band in the mid-IR region (c) [**P4**].

crystals from the background impurities [**P6**].

At the same time, doping with ytterbium leads to appearance of a new band with the maximum at $\sim$ 1.6 μm in the spectra of ZnSe:Yb [I] crystals (Fig. 17-b and -c). This band was not previously observed in spectra of intrinsic crystals or crystals doped with TM. The intensity of the band quickly decreases with increasing temperature, and at temperatures above 100 K (Fig. 17-c) the band could hardly be observed on the background of the $\sim$ 2 μm band. A band with similar properties is also observed in the same spectral region of the ZnSe:Yb [Bi] crystals PL spectra (Fig. 18-b and -c)). Addition of Yb impurity to the Bi melt during annealing process leads to disappearance of the band with maximum at $\sim$ 1.5 μm, attributed to the bismuth emission centers [116]. Instead of this band in spectra of ZnSe:Yb [Bi] crystals, a band with maximum at $\sim$ 1.7 μm may be observed. Increase of the Yb concentration in the Bi melt leads to the decrease of the band intensity (Fig. 18-b). This emphasizes the similarity with the $\sim$ 1.6 μm band in spectra of ZnSe:Yb [I] crystals, which disappears at large Yb concentration (Fig. 17-b). The complicated dependence of the bands intensity on the Yb concentration is another argument in favor of the assumption that Yb impurity tends to form some complexes or clusters. Also, this emission band one more time emphasizes the similarity of the Yb influence on the PL spectra of ZnSe:Yb [I] and ZnSe:Yb [Bi] crystals.

Structured bands in the near-IR spectral range (Fig. 18-a, Fig. 19-a) are character-

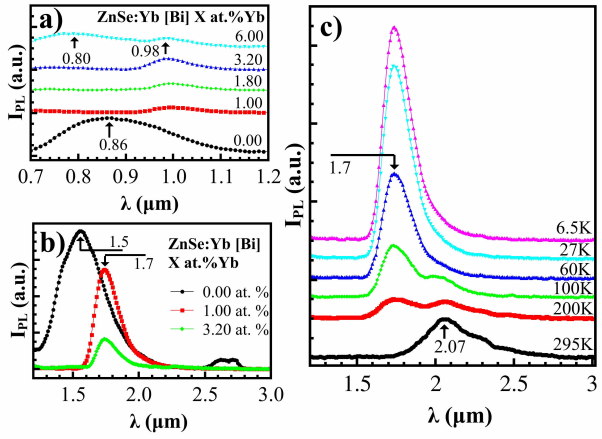

Figure 18: PL spectra of ZnSe:Yb [Bi] crystals in near-IR (a) and mid-IR (b) regions at T=6.5 K. The temperature evolution of the ZnSe:Yb [Bi] 1.00 at. % PL band in the mid-IR region (c) [**P4**].

istic for the Yb doped crystals [26, 30, 32]. Emission with the maximum at 0.98 μm is usually associated with intrashell transitions between the ground ($^2F_{7/2}$) and exited ($^2F_{5/2}$) states of the Yb^{3+} ions [26, 30]. The temperature dependence of this maximum (Fig. 19-c) confirms the intrashell character of the emission. The presence of this characteristic band indicates the incorporation of the ytterbium impurity in the crystal lattice in the form of Yb^{3+} ions. Increase of the 0.98 μm maximum contribution to the spectra, with increase of the ytterbium concentration in the doping media, confirms the conclusion made. However, it should be mentioned that the intensity of the Yb intrashell emission is much higher in the crystals doped by annealing in the zinc melt. This supports the conclusion made during discussion of the visible PL spectra about more significant influence of the Yb on emission properties of the crystals, when concentration of the selenium vacancies is higher.

The presence of an additional band, overlapping the ytterbium ions' intrashell emission from the shorter wavelengths part of the band, was also previously observed [26]. Usually this band is explained by trapping of the hole from the valence band by the Coulomb-attractive potential provided by the ytterbium compensating ion with a further charge-transfer resulting in excitation of REE ion [30]. Thus, the different spectral position of the maximum, overlapping Yb^{3+} ions intrashell emission in ZnSe:Yb [Zn] and ZnSe:Yb [Bi] crystals (Fig. 18-a, Fig. 19-a), is caused by different compensation mechanisms of the REE ions.

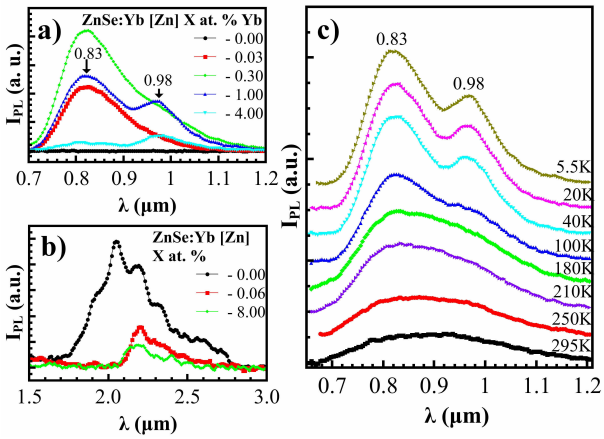

Figure 19: PL spectra of ZnSe:Yb [Zn] crystals in near-IR (a) and mid-IR (b) regions at T=6.5 K. The temperature evolution of the ZnSe:Yb [Zn] 1.00 at. % PL band in the mid-IR region (c) [**P4**].

In the mid-IR spectral range of the ZnSe:Yb [Zn] crystals' PL spectra (Fig. 19-b) a band, similar to the one earlier seen in the ZnSe:Yb [I] emission spectra ((Fig. 17-b), can be observed. This can be explained by the uncontrolled contamination of the source material. The intensity of this band is 30 times smaller than of the intrashell emission of the Yb ions and decreases with increase of the ytterbium impurity concentration in the doping melt. Decrease of the 2 μm band was also observed at high concentration of the Yb ions in ZnSe:Yb [I] crystals, which may be considered as a sign of a cluster formation on the basis of ytterbium impurity and uncontrolled background defects.

4.2 Optical density

The optical density spectra for all studied ZnSe:Yb crystals are presented in Fig. 20. The sharp decrease in transparency below $\sim$ 500 nm is caused by intrinsic absorption of ZnSe, however, any significant absorption lines were not observed in the whole studied spectral range. This result confirms assumption about indirect excitation of the center based on Yb^{3+} ion. A characteristic for all studied spectra is decrease of optical density with increasing Yb concentration in the crystals. Similarity of technological processes within the crystal series allows to exclude possibility of the extraction of the uncontrolled background impurities into the growth media. It may be assumed that increase of the samples transparency is caused by inclusion of the singular impurities in clusters. Thus, internal light dispersion should be smaller, which may result in the observed

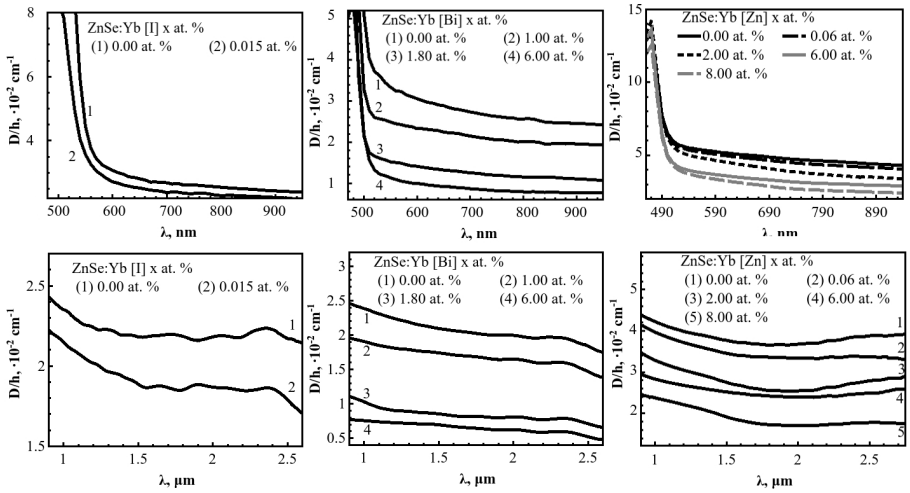

Figure 20: Optical density spectra of ZnSe:Yb crystals, T = 300 K [unpublished].

decrease of the optical density. However, presence of the large impurity blocks in the crystal lattice should lead to the significant decrease in the crystals transparency in the far-IR range.

4.3 Electrical properties

4.3.1 ZnSe:Yb

The behaviour of the Hall temperature dependence may be explained with the "impurity band" model [117–120]. Increase of the Yb concentration leads to the increase of the relative amplitude of the observed maximum (Fig. 21-a). This fact is a vivid manifestation of "purification" of ZnSe:Yb [Zn] samples during the doping with REEs from uncontrolled background impurities that form the impurity band. Ytterbium atoms are incorporated into the ZnSe crystal lattice and bind shallow impurities in electrically passive complexes. Finally, the concentration of single centers of background impurities, which form the impurity band, decreases. This conclusion is in a good agreement with photoluminescent data (see section 4.1), where the formation of the Yb-based complexes was also shown.

The relatively small value of the maximum in the $R_H(T)$ dependence for the undoped n-ZnSe [Zn] sample (Fig. 21-a, curve 1), its highest-temperature position and the well-manifested constancy of the Hall coefficient at low temperatures ($T < 30$ K) are the evidence of the well-developed, fairly wide impurity band, which is located near the

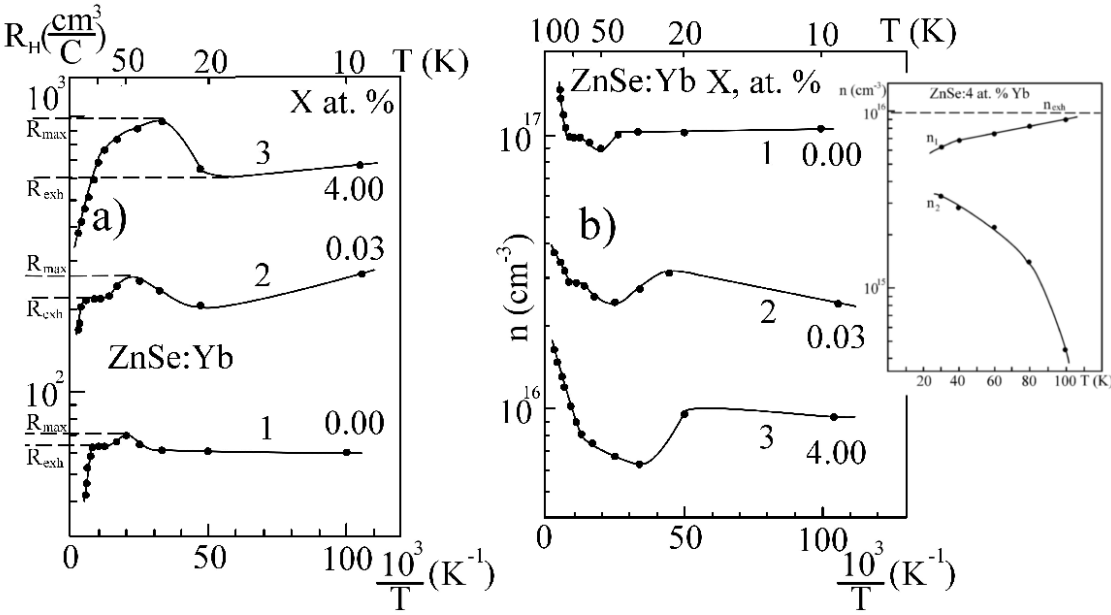

Figure 21: Temperature dependence of the Hall coefficient (a) and of the free electron concentration (b) for n-ZnSe:Yb [Zn] samples with various dopant concentrations. Inset: Temperature dependence of the free electron concentrations in the conduction band (n_c) and the impurity band (n_b) for n-ZnSe:4 at.% Yb sample [**P6**].

conduction band minimum but not overlapping with it.

Manifestation of a small slope on the R_H dependence for ZnSe:Yb [Zn] samples at $T < 20$ K is also a result of the sample "purification" from background impurities, which is accompanied by decreasing of the bandgap energy, appearance of the impurity density-of-states tails due to their random distribution and electron freeze-out from the impurity band into these local states.

The increase of sample temperature from 150 to 300 K leads to a rapid decrease of the Hall coefficient due to ionization of deep impurity level of unknown origin.

The temperature dependence of the Hall coefficient in the temperature range, where the impurity conductivity should be absent ($T \geq 50$ K) and electronic gas in the studied samples is not degenerated, makes it possible to determine the concentration of shallow donors, N_D, concentration of acceptors, N_A, and activation energy of donor impurity, E_D, using the equation [121]

$$\frac{n\,(N_A + n)}{(N_D - N_A - n)} = \frac{2\left(\frac{2\pi m^* k_B T}{h^2}\right)^{3/2}}{g} \exp\left(\frac{-E_D}{k_B T}\right), \qquad (10)$$

where g is the degeneracy of the donor state and m^* is the electron effective mass. The values of the parameters calculated by least-square fitting of the experimental data to Eq. (10) show that introduction of ytterbium atoms into ZnSe [Zn] crystals considerably reduces the concentrations of both electrically active shallow donors and acceptors, as a part of them enters into the composition of neutral complexes formed near the ytterbium atoms.

The temperature dependence of free electron concentration, n, in the temperature range that corresponds to activation of deep impurity level is described by the equation [121]

$$\frac{n\left(n-n_0\right)}{\left(N_{\mathrm{Deep}}+n_0-n\right)}=\frac{2\left(\frac{2\pi m^* k_B T}{h^2}\right)^{3/2}}{g_1}\exp\left(\frac{-E_{\mathrm{Deep}}}{k_B T}\right), \tag{11}$$

where N_{Deep} is the concentration of deep donors, E_{Deep} is the ionization energy, n_0 is the concentration of the electrons activated from shallow donors in the region of their exhaustion and g_1 is the degeneracy of the deep level.

The temperature dependence of the electrical conductivity, σ, presented in Fig. 22, is almost completely determined by the temperature dependence of the free electron concentration (Fig. 21-b), as the electron Hall mobility, $R_H\sigma$, weakly depends on temperature (Fig. 22 inset). Figure 22 shows that the doping of ZnSe [Zn] samples with Yb impurity increases the electrical conductivity in the whole investigated temperature range, and this increases with increase of Yb impurity concentration, while the concentration of free electrons decreases (Fig. 21-b). The reason for growth of electrical conductivity with decreasing concentration of free electrons is a significant increase (about an order of magnitude, see Fig. 22 inset) of electron mobility due to "purification" of the samples from single background impurities, which are effective centers for charge carrier scattering.

For the sample with the highest concentration of Yb impurity (Fig. 22 inset), curve 3), the electron mobility in the temperature range from 100 to 300 K obeys the $T^{-3/2}$ law, thus, the scattering of free charge carriers by acoustic phonons takes place. This result is in good correlation with the change of electrical conductivity at $T > 100$ K (Fig. 22, curve 3), which appears due to "purification" of the sample from background impurities.

The simplest and the most evident method for analyzing the energy level spectrum for the crystals with impurity band is based on the study of temperature dependence of the Fermi level, μ_F. This dependence for all the investigated samples was calculated according to the equation [122]

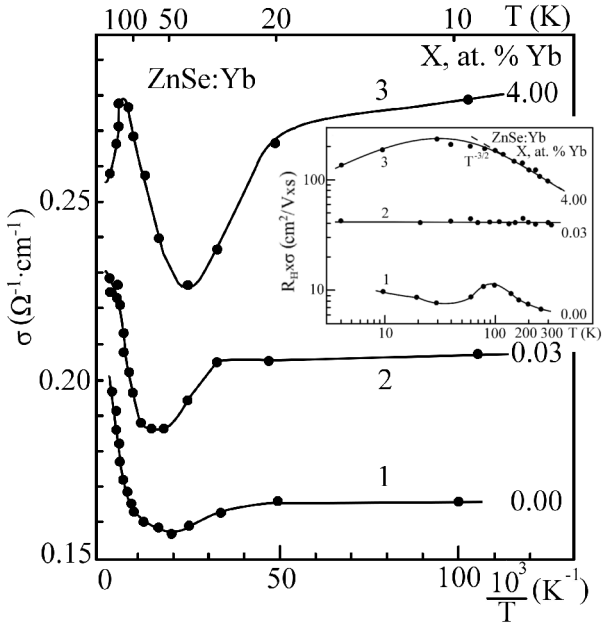

Figure 22: Temperature dependence of the electrical conductivity and the electron Hall mobility (inset) of n-ZnSe:Yb [Zn] samples with various dopant concentrations [**P6**].

$$n_c\left(T\right) = 4\pi\left(\frac{2m^*k_BT}{\hbar^2}\right)^{3/2} F_{1/2}\left(\mu_F^*\right) = 5.45\cdot 10^{15}\left(m^*\right)^{3/2} T^{3/2} F_{1/2}\left(\mu_F^*\right) \quad (12)$$

where n_c is the electron concentration in the conduction band, $\mu_F^* = \mu_F/k_BT$ is the reduced Fermi level and $F_{1/2}(\mu_F^*)$ is the Fermi integral, the values of which are tabulated [123].

For the calculation of the temperature dependence of the Fermi level, the temperature dependence of the free electron concentration n_c is needed. The $n_c(T)$ and $n_b(T)$ dependences, where n_b is the concentration of electrons in the impurity band, may be calculated using a two-band semiconductor model. The results of this calculation are given in Fig. 21 (inset) for the ZnSe:4 at.% Yb sample. Then, using the equation (12), the temperature dependence of the Fermi level, $\mu_F(T)$, (Fig. 23-a) and the reduced Fermi level, $\mu_F^*(T)$, (Fig. 23-b) were calculated.

The temperature dependence of the reduced Fermi level (Fig. 23-b) shows that as the Yb dopant concentration increases, the temperature of the beginning of electron gas degeneracy ($\mu_F^* = 0$) shifts towards low temperatures and the degree of electron gas

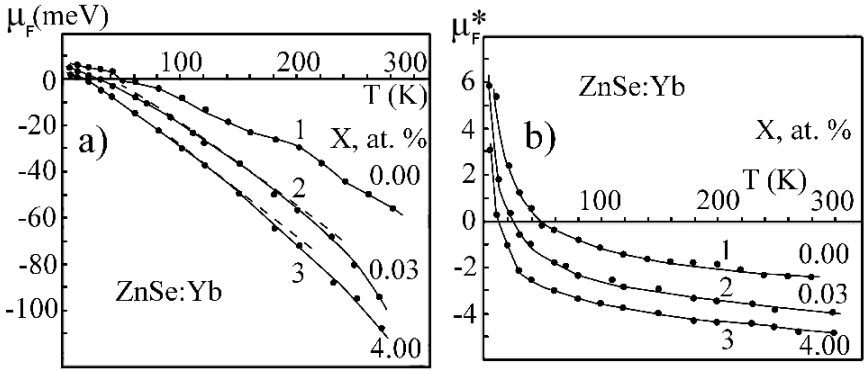

Figure 23: Temperature dependence of the Fermi level (a) and reduced Fermi level (b) for n-ZnSe:Yb [Zn] samples [**P6**].

degeneracy decreases. This effect is a consequence of "purification" of the investigated ZnSe:Yb [Zn] samples from electrically active background impurity.

4.3.2 ZnSe:Gd

Concentration of the free electron charge carriers in the undoped sample from the ZnSe:Gd [Zn] series is even higher than in the similar sample from the ZnSe:Yb [Zn] series. This is caused by selection of another initial ZnSe crystal crystal for sample preparation. Concentration of the free electron charge carriers in the undoped sample is $n = 1.8 \cdot 10^{20}$ cm^{-3} and changes non-linearly with the temperature and concentration (Fig. 24-a), the fact also observed for the ZnSe:Yb [Zn] samples (Fig. 24-b).

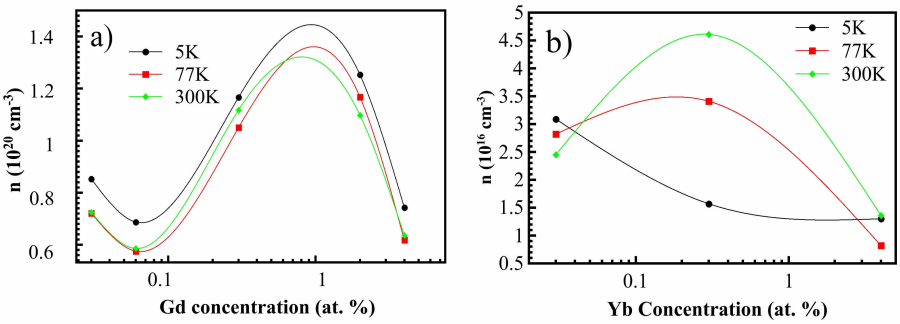

Figure 24: The dependence of the free electron concentration on the Gd (a) and Yb (b) impurity concentration (curves are drawn by eye)[unpublished].

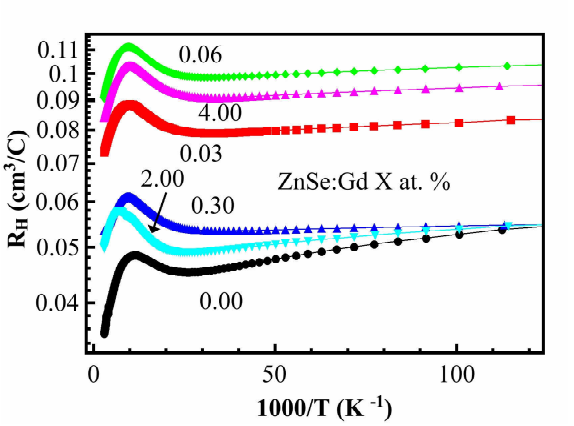

Figure 25: Temperature dependence of the Hall coefficient for n-ZnSe:Gd [Zn] samples [unpublished].

The temperature dependence of the Hall coefficient of the ZnSe:Gd [Zn] crystals (Fig.25) has a similar shape as the dependence of ZnSe:Yb [Zn] crystals. A maximum characteristic for the impurity band is observed, also, for Gd series it is shifted to the higher temperatures ($\sim$ 100 K) comparing to the Yb series ($\sim$ 40 - 50 K). It may be assumed that at such a high free charge concentration the impurity band formed by donors with the small activation energy overlapps with the conduction band. At the same time, another impurity band is formed in the ZnSe:Gd [Zn] crystals by the deep donors, presence of which was univocally established for the ZnSe:Yb [Zn] because of their thermal activation at $\sim$ 200 - 300 K. The temperature dependence of the charge carriers Hall mobility for the ZnSe:Gd [Zn] confirms the impurity band model (Fig.

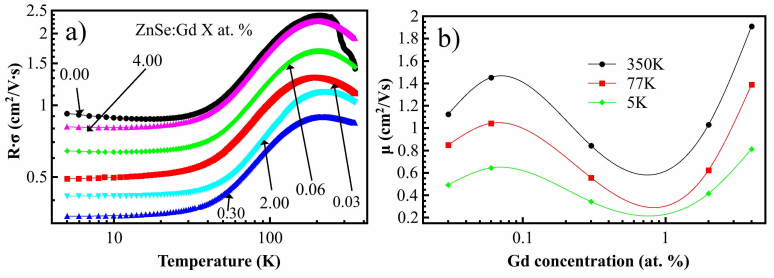

Figure 26: Temperature (a) and Gd concentration (b) dependence of Hall mobility for n-ZnSe:Gd [Zn] samples [unpublished].

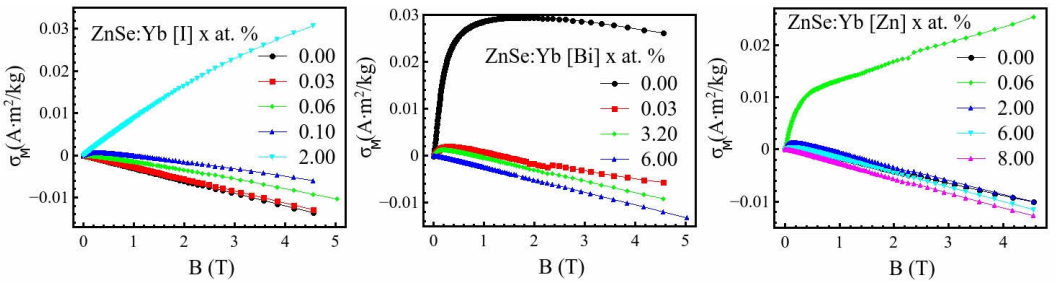

Figure 27: Field dependence of mass-magnetization of ZnSe:Yb crystals, T = 5 K [unpublished].

26-a).

Presence of a maximum in the temperature dependence of the Hall mobility shows the presence of charge scattering on phonons (for $T > T_{max}$) and impurity ions (for $T < T_{max}$). A sharp decrease of the electron mobility at 30 - 40 K represents a transition to conductivity within the impurity band. Reduced values and unsignificant temperature dependence are characteristic for the electron mobility within the impurity band.

4.4 Magnetic properties

The change of the magnetic properties of the samples with increasing Yb concentration significantly depends on the doping method (Fig. 27). In the case of the iodine co-doped samples increase of Yb concentration leads to increase of paramagnetic signal, which may arise from the iodine complexes. In case of the bismuth co-doped the situation is opposite increase of Yb concentration leads to increase of diamagnetic signal, which is most probably caused by the ZnSe host, thus ytterbium influence results in approaching of magnetic properties of doped ZnSe:Yb [Bi] crystals to the properties of intrinsic ZnSe samples, but with smaller concentration of native and uncontrolled impurity defects (more perfect). The case when the crystals were doped from the zinc melt represents combination of the two previously discussed cases. This behavior of the magnetic properties with increase of the Yb impurity may be explained by formation of Yb-based complexes, when magnetic moments of defects, which are joined by Yb in complex, are compensated. Thus magnetic properties will be controlled not by Yb itself but by combination of Yb and other defects.

4.5 Structure of the impurity center

The emission properties indicate that selenium vacancies are involved in the Yb doping. Optical and electrical measurements allow observing decreasing concentration of singular defects, when REE ion concentration in the samples increases. From the electrical properties a simultaneous compensation of both acceptor and donor defects was seen. Magnetic properties show that Yb impurity forms complexes. All these facts may be combined together within the slightly modified Brown's model [32]. An ionized selenium vacancy creates +2e charge. Placement of a triple charged REE ion in it increases charge to +5e. Charge compensation may be achieved by substitution of the first order neighbours of Yb^{3+} , $4Zn^{2+}$ ions in tetrahedron nodes, by singly charged ions. In such a case, a cluster based on REE ion surrounded by four singly charged ions is formed. The total charge of such a cluster will be +e and its formation is accomplished by simultaneous compensation of both donor and acceptor impurities.

5 Influence of d- and f-elements co-doping on emission properties of ZnSe crystals

The luminescent properties of ZnSe, ZnSe:Cr (0.05 at.% Cr), ZnSe:Yb (0.03 at.% Yb) and ZnSe:Cr:Yb (0.05 at.% Cr, 0.05 at.% Yb) crystals, doped during the growth process by the chemical vapor transport method, were compared within the temperature interval of 6 - 300 K. The emission spectra of Cr and Yb doped crystals are discussed in details in sections 3.1.1 and 4.1, respectively. Thus, only the spectra of d- and f- ions co-doped samples will be analysed here.

Co-doping of the zinc selenide crystals with chromium and ytterbium leads to combined influence of these impurities on the edge band emission (Fig. 28). The position of the edge-band maximum in the PL spectrum shifts to the more short-wavelength region comparing to the undoped sample or samples doped with a single type of impurity. Energy position (439.5 nm) of the bands maximum in the PL spectrum of TM and REE co-doped crystal is in good agreement with the zinc selenide band-gap at the liquid helium temperature[18] allowing the conclusion that the emission is caused by CB - VB radiative transitions. The thermal band-gap expansion coefficient at temperatures above 80 K ($dE_g/dT = 45 \cdot 10^{-4}$ eV/K), similar to that given by the other authors [124], agrees with this conclusion. At the same time, the similarity of the band-gap thermal expansion coefficient between the samples excludes the possibility of phase separation and formation of solid solutions due to the doping. Absence of the observable exciton emissions is caused by the presence of significant internal fields in the crystals, which prevent the exciton formation. The decrease of the edge-band intensity is similar to that observed in the ZnSe:Cr PL spectrum, however, differences in the temperature quenching activation energies [**P7**] indicate differences in the electronic transitions in the co-doped crystal and crystals doped only with TM or REE impurity.

In the IR spectral range co-doping of the zinc selenide crystals with chromium and ytterbium impurities leads to appearance of a large band with nearly constant intensity within 1.6 μm - 2.4 μm spectral interval (Fig. 28). This band retains the complex structure observed earlier in ZnSe:Cr samples, and also has an additional maximum localized close to 1.7 μm. Energy position of the 1.7 μm maximum is in a good agreement with the energy distance between Cr^{+} and Cr^{2+} ions levels within the zinc selenide band-gap. This allows us to conclude the possibility of light emission transitions between two neighboring chromium ions in different charge states. It is also worth mentioning, that the high energy part of this band may have a similar origin as the 1.6 μm band,

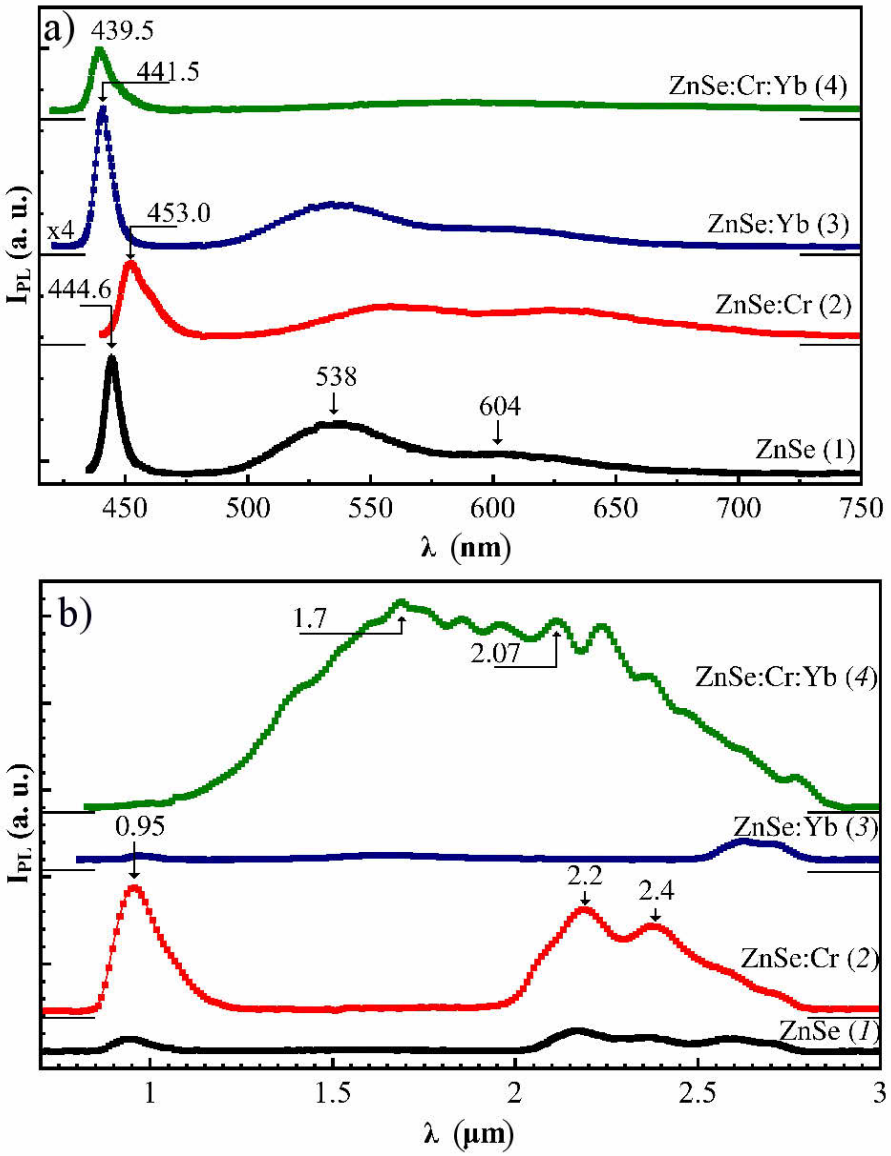

Figure 28: PL spectra of ZnSe (1), ZnSe:Cr (2), ZnSe:Yb (3) and ZnSe:Cr:Yb (4) crystals in the visible (a) and IR (b) spectral range at T = 6.5 K [**P7**].

previously observed in spectra of ZnSe:Yb crystals (see section 4.1).

The Cr^+ ions represent a non-equilibrium state in ZnSe, however, as it was described in section 4.5, ytterbium ion requires a charge compensation, which may be achieved by substitution of the first order neighbours by single charged ions. In the case of the ZnSe:Cr:Yb crystals the ytterbium ion, most probably, stabilizes the singly charged chromium ions in the zinc crystal lattice nodes by the analogy with the Brown model [32]. In such a case, resonant energy transfer from one chromium ion to another will not lead to the concentration quenching as in the case of ZnSe:Cr crystals (see 3.1.1), but to the broadening of the complex IR band, as observed in the ZnSe:Cr:Yb crystals PL spectrum.

Based on the described model it may concluded that co-doping of the ZnSe crystals with ytterbium and chromium will lead to the change of the chromium ion equilibrium charge state: the dominant charge state without excitation is Cr^+ in ZnSe:Cr:Yb crystals and Cr^{2+} in ZnSe:Cr. However, both charge states should be observed under the laser excitation [51], but the electron transitions will significantly differ. Despite the fact that chromium concentration in both samples ZnSe:Cr and ZnSe:Cr:Yb is the same, the structure of the spectra is completely different. The band in the near-IR spectral range with maximum close to 0.95 μm observed in spectra of ZnSe:Cr crystal disappears in the spectra of co-doped sample. This may be explained by the electron transitions involved in formation of the discussed band. In PL spectrum of the ZnSe:Cr sample the 0.95 μm band appears because of the intra-shell transitions between second excited ($^3T_1$) and ground ($^5T_2$) states of the Cr^{2+} ion [89]. In ZnSe:Cr:Yb crystal, when an electron will be placed on the external shell of non-equilibrium Cr^{2+}, it will have a much higher probability to be taken away from the ion than in the case of ZnSe:Cr crystal. In ZnSe:Cr crystals, when Cr^{2+} is equilibrium charge state, electron most probably will relax to the ground ($^5T_2$) state of Cr^{2+} ion emitting a photon in near-IR spectral region. However, it was shown [**P1**] that electron transitions responsible for 0.95 μm band in ZnSe:Cr crystals are competitive with transitions responsible for 2.07 μm band. At $T \sim 5$ K the intensity of the band in near-IR region is higher than the intensity of the band at 2.07 μm [**P1**]. Temperature increase leads to the quenching of the 0.95 μm band and the increase of the mid-IR band intensity. In the case of the ZnSe:Cr:Yb crystals, a similar situation may be observed, but instead of $^3T_1 \rightarrow {}^5T_2$ transitions within Cr^{2+} ions, recharge transitions between Cr^{2+} and Cr^+ ions are involved (Fig. 29). The temperature dependence of the IR broad band in the PL spectrum of ZnSe:Cr:Yb crystal confirms participation of chromium ions in formation of both 1.7 μm and 2.07 μm components.

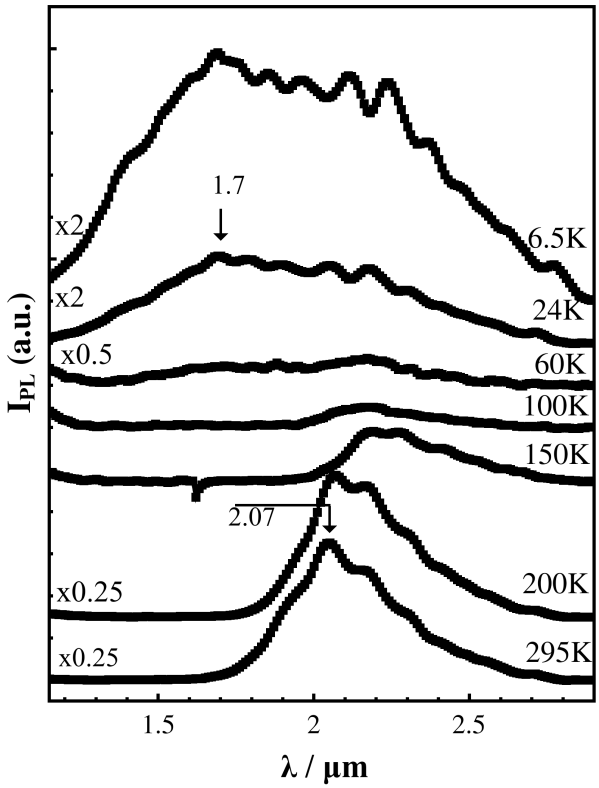

Figure 29: Temperature evolution of the IR band in the PL spectrum of ZnSe:Cr:Yb crystal [**P7**].

It is known that the efficiency of the intrashell emission caused by $^5E \rightarrow {}^5T_2$ transitions within Cr^{2+} ions is higher at room temperature than at lower temperatures [86, 88]. This may indicate that at room temperature the IR emission of the ZnSe:Cr crystals is formed as the result of $Cr^{2+} \rightarrow (Cr^{2+})^* \rightarrow Cr^{2+}$ transitions. At low temperatures, IR emission may be formed because of transition with participation of the semiconductor allowed bands, which requires changing of the chromium ion charge state [51]. It also may be supposed that at higher temperatures the probability to change the charge state of equilibrium Cr^+ ions, which appears because of formation of ytterbium cluster, is lower, and this lowers the probability of transitions responsible for the 1.7 μm emission.

6 Conclusions

In this thesis influence of d- and f-elements on emission, optical, electrical and magnetic properties of ZnSe were investigated within a wide temperature range (5 - 300 K). Doping was performed by various technological methods that allowed to study interaction between doping impurities of Cr, Ni, Yb and Gd and the most common uncontrolled contamination impurities and native defects.

It was shown that only 2+ ions of the d-element are optically active and give rise to emission bands in the visible and IR spectral ranges. It was proved that broad emission bands in the mid-IR spectral range, attractive from application point of view, are caused by the resonance energy transfer between the doping ions and background native and impurity defects. Also, it was shown that the intensity and the structure of the emission bands are determined not only by the impurity type and its concentration but also by the initial concentration of the native defects, thus, a combination of different impurities and doping techniques may allow to extend the tunability range of the possible laser systems.

The performed study allows to assume that simultaneous usage of both optical and magnetic properties of TM doped ZnSe crystals in practical applications may be difficult, because the highest emission efficiency from the crystal may be obtained at low concentration of d-ions, when magnetic properties exhibited by them are weak and comparable by the value with crystal host or uncontrolled defects magnetism. High concentration of the TM doping impurity may be interesting for some magnetic applications, however, the magnetic interaction between d-ions leads to quenching of the emission and significant decrease in optical transparency. Thus, it was established that the effect of concentration quenching of the emission observed for the ZnSe:TM crystals is most probably caused by magnetic coupling of emission centers and changing of its structure.

Doping of ZnSe with REE results in decrease of concentration of singular defects in the crystals. This leads to simultaneous compensation of donor and acceptor defects, which may be a key for obtaining of p-type conductivity in bulk zinc selenide. It was shown that co-doping of ZnSe with Yb ion and selenium substituting impurities, which decrease concentration of selenium vacancies, results in weak influence of ytterbium on the emission spectra. On the other hand, annealing of the crystals in Zn+Yb melt, which favors the generation of selenium vacancies, leads to appearance of intensive band in the near-IR range, characteristic for the ytterbium doped crystals. It was established that the increase of Yb ion concentration leads to the destruction of the complexes, which include selenium vacancies. These facts allow us to conclude that selenium vacancies

are directly involved in formation of Yb-based emission centers by increasing the ytterbium ions solubility in ZnSe crystals or by formation of complexes with ytterbium ions.

It was shown that co-doping of zinc selenide with the TM and REE impurities leads to the combination of their influence on the crystal's emission, being a powerful tool for modeling of required properties for practical applications.

The research carried out in this thesis has shown that all studied properties of zinc selenide crystals are determined not by the doping impurity exclusively but by interaction between native and impurity defects. Control over the concentration of the intrinsic defects is a big challenge for all II-VI semiconductor compounds and sometimes is crucial for practical applications. However, it is evident that nanostructuring will lead to significant increase in concentration of the surface defects comparative to the concentration of the native defects in volume, thus, allowing to control concentration of the intrinsic defects by changing the size of the particle. It allows to think that nanostrucuring will give possibility to change concentration of native and impurity defects independently and to control interaction between them. As it was shown in the thesis, namely this interaction mainly determines the crystal properties. A logical continuation of the presented work will be study of the physical properties of nanostructured II-VI semiconductor compounds doped with transition metals and rare-earth elements, for which control over interaction between native and impurity defects seems to be less complicated.

References

[1] Joachim Piprek, *Semiconductor Optoelectronic Devices* (Academic Press, California, USA, 2003).

[2] Manuel Aven and Jerome S. Prener, *Physics and Chemistry of II-VI Compounds* (North-Holland, Amsterdam, 1967), 862 pp.

[3] Klaus Irmscher and Michael Prokesch, Materials Science and Engineering B **80**, 168–172 (2001).

[4] Bernard Valeur and Mario N. Berberan-Santos, J.Chem.Educ. **88**, 731 (2011).

[5] P. P. Feofilov, Sov. Phys. Usp. **4**, 770 (1961).

[6] S. Kasap and P. Capper, *Springer Handbook of Electronic and Photonic Materials* (Springer US, 2007).

[7] H. A. Klasens, J. Electrochem. Soc. **100**, 72 (1953).

[8] John Lambe and Clifford C. Klick, Phys. Rev. **98**, 909 (1955).

[9] E. F. Apple and F. E. Williams, J. Electrochem. Soc. **106**, 224 (1959).

[10] C. S. Hung and J. R. Gliessman, Phys. Rev. **79**, 726 (1950).

[11] C. S. Hung, Phys. Rev. **9**, 727 (1950).

[12] Hubert M. James and Arthur S. Ginzbarg, J. Phys. Chem. **57**, 840 (1953).

[13] H. Fritzsche, Phys. Rev. **99**, 406 (1955).

[14] S. Blundell, *Magnetism in Condensed Matter* (Oxford University Press, New York, 2001).

[15] A. Lewicki, A. I. Schindler, J. K. Furdyna, and W. Giriat, Phys. Rev. B **40**, 2379 (1989).

[16] Akira Narita, J. Phys. C: Solid State Phys. **19**, 4797 (1986).

[17] A. Bonanni and T. Dietl, Chem. Soc. Rev. **39**, 528 (2010).

[18] T.S. Moss and S. Mahajan, *Handbook on semiconductors. Vol. 3. Materials, Properties and Preparation* (Elsevier Science, North-Holland, Amsterdam, 1994).

[19] S. Ibuki *et al.*, J. Lumin. **1,2**, 797 (1970).

[20] A. F. J. Cox and W. A. Shand, J. Phys. C: Solid State Phys. **4**, 2962 (1971).

[21] G.J. Goldsmith, S. Larach, R.E. Shrader, and P.N. Yocom, Sol. State Communic. **1**, 25 (1963).

[22] W. W. Anderson, Phys. Rev. **136**, 556 (1964).

[23] R. Boyn, Phys. Stat. Sol. (b) **148**, 11 (1988).

[24] M. R. Brown, A. F. J. Cox, W. A. Shand, and J. M. Williams, J. Phys. C: Solid St. Phys. **4**, 1049 (1971).

[25] Hiroyoshi Komiya, J. Phys. Soc. Japan **24**, 216 (1968).

[26] Irena Szczurek and Henryk Lozykowsky, J. Lumin. **14**, 389 (1976).

[27] Hiroyoshi Komiya, J. Phys. Soc. Japan **23**, 666 (1967).

[28] R.K. Watts, Sol. State Comm. **4**, 549 (1966).

[29] R. K. Watts and W. C. Holton, Phys. Rev. **173**, 417 (1968).

[30] H. Przybylinska *et al.*, Phys. Rev. B **40**, 1748 (1989).

[31] J. D. Kingsley and M. Aven, Phys. Rev. **155**, 235 (1967).

[32] M. R. Brown, A. F. J. Cox, W. A. Shand, and J. M. Williams, J. Phys. C: Solid St. Phys. **4**, 2550 (1971).

[33] Hiroyoshi Komiya, J. Phys. Soc. Japan **27**, 893 (1969).

[34] Herbert A. Weakliem, J.Chem. Phys. **36**, 2117 (1962).

[35] T.P. Surkova *et al.*, Physica B **273-274**, 848 (1999).

[36] A. Twardowski *et al.*, J. App. Phys. **73**, 5745 (1993).

[37] W. Mac *et al.*, Phys. Rev. B **50**, 14144 (1994).

[38] S. F. Dubinin *et al.*, Physics of the Solid State **50**, 1087–1090 (2008).

[39] H. Saito *et al.*, J. App. Phys. **91**, 8085 (2002).

[40] Yu. A. Nitsuk, Semicond. **47**, 736 (2013).

[41] G. Grebe, G. Roussus, and H.-J. Schulz, J. Lumin. **12/13**, 701 (1976).

[42] U. Hömmerich, I.K. Jones, Ei Ei Nyein, and S.B. Trivedi, J. Cryst. Growth **287**, 450 (2006).

[43] N. Vivet, J.L. Doualan, M. Morales, and M. Levalois, J. Lumin. **130**, 1449 (2010).

[44] M. Godlewski, M. Surma, V. Yu. Ivanov, and T. Surkova, Low Temp. Phys. **30**, 891 (2004).

[45] Laura D. DeLoach *et al.*, IEEE Journal of Quantum Electronics **32**, 885 (1996).

[46] Maria C. Tamargo, *II-VI Semiconductor Materials and their Applications* (Taylor and Francis, New York, 2002).

[47] J. V. Van Vechten, Phys. Rev. **182**, 891 (1969).

[48] E. M. Gavrushchuk, Inorganic Materials **39**, 883 (2003).

[49] B. K. Vainshtein, *Modern Crystallography* (Springer-Verlag Berlin, 1994).

[50] R. D. Shannon, Acta Crystallographica Section A **32**, 751 (1976).

[51] V.V. Fedorov, A. Gallian, I. Moskalev, and S.B. Mirov, J. Lumin. **125**, 184 (2007).

[52] S. Mirov *et al.*, J. Lumin. **133**, 268 (2013).

[53] Cornelia Fischer, Evgeni Sorokin, Irina T. Sorokina, and Markus W. Sigrist, Optics and Lasers in Engineering **43**, 573 (2005).

[54] Kazi Sarwar Abedin *et al.*, Appl. Opt. **37**, 1642 (1998).

[55] Jerome Faist *et al.*, Science **264**, 553 (1994).

[56] Julien Jaeck *et al.*, Opt. Lett. **31**, 3501 (2006).

[57] Alphan Sennaroglu, Umit Demirbas, Adnan Kurt, and Mehmet Somer, IEEE Journal of Selected Topics in Quantum Electronics **13**, 823 (2007).

[58] J. Kreissl and H.J. Schulz, J. Cryst. Growth **161**, 239 (1996).

[59] A. Burger *et al.*, J. Cryst. Growth **225**, 249 (2001).

[60] J. T. Vallin, G. A. Slack, S. Roberts, and A. E. Hughes, Phys. Rev. B **2**, 4313 (1970).

[61] M. E. Doroshenko *et al.*, Laser Phys. Lett. **4**, 503 (2007).

[62] A. V. Podlipensky *et al.*, Appl. Phys. B **72**, 253 (2001).

[63] Georges Boulon, Opt. Mater. **34**, 499 (2012).

[64] Antoine Godard, C. R. Physique **8**, 1100 (2007).

[65] S. Chenais *et al.*, Opt. Mater. **22**, 99 (2012).

[66] Tso Yee Fan *et al.*, IEEE J. Select. Topics Quant. Electr. **13**, 448 (2007).

[67] Shu-min Zhang, Fu-yun Lu, and Jian Wang, Opt. Comun. **263**, 47 (2006).

[68] J. Y. Huang *et al.*, Optics express **16**, 3002 (2008).

[69] J.F. Philipps *et al.*, Appl. Phys. B **72**, 399 (2001).

[70] M. Llusca *et al.*, Thin Solid Films **562**, 456 (2014).

[71] Benxue Jiang *et al.*, Opt. Mater. **29**, 1188 (2007).

[72] Xiaodong Xu *et al.*, Mater. Sci. Eng. B **117**, 17 (2005).

[73] W. Mac *et al.*, Phys. Rev. Lett. **71**, 2327 (1993).

[74] X. L. Wang *et al.*, App. Phys. Lett. **102**, 102112 (2013).

[75] O. V. Koplak *et al.*, Physics of the Solid State **55**, 1870 (2013).

[76] H. Schäfer, *Chemische Transportreaktionen* (VCH Verlag GmbH, 1962).

[77] K. Böttcher and H. Hartmann, J. Cryst. Growth **146**, 53 (1995).

[78] K.H.J. Buschow, *Magnetic and superconducting materials* (Amanda Weaver, 2005).

[79] A. Fazzio, M. J. Caldas, and Alex Zunger, Phys. Rev. B **30**, 3430 (1984).

[80] J. P. Varshni, Physica **34**, 149 (1967).

[81] S. Bhaskar *et al.*, J. App. Phys. **85**, 439 (1999).

[82] J. R. Haynes, Phys. Rev. Lett. **17**, 860 (1966).

[83] J. R. Haynes, Phys. Rev. Lett. **4**, 361 (1960).

[84] R. E. Halsted and M. Aven, Phys. Rev. Lett. **14**, 64 (1965).

[85] V. Gavryushin, A. Kadys, M. Sudzius, and K. Jarasiunas, JETP Letters **83**, 22 (2006).

[86] M. Godlewski, A. J. Zakrzewski, and V. Yu. Ivanov, J. Alloys Compd. **303-301**, 23 (2000).

[87] R. N. Bhargava, R. J. Seymour, B. J. Fitzpatrick, and S. P. Herko, Phys. Rev. B **20**, 2407 (1979).

[88] M. Surma and M. Godlewski, Radiat. Eff. Defects Solids **135**, 213 (1995).

[89] M U Lehr *et al.*, J. Phys. Cond. Mat. **9**, 753–763 (1997).

[90] Yiqun Shen *et al.*, Sol. Stat. Electr. **52**, 1833 (2008).

[91] Yi-Yang Zhou and Fu-Zhen Li, J. Phys. Chem. Solids **59**, 1105 (1998).

[92] D.D. Nedeoglo *et al.*, Physica B **406**, 3851–3855 (2011).

[93] Vladimir A. Fonoberov *et al.*, Phys. Rev. B **73**, 165317(9p.) (2006).

[94] T. Schmidt, K. Lischka, and W. Zulehner, Phys.Rev.B **45**, 8989 (1992).

[95] Leah Bergman *et al.*, J.Appl.Phys **96**, 675 (2004).

[96] Huanyong Li, Wanqi Jie, and Kewei Xu, Journal of Crystal Growth **279**, 5 (2005).

[97] B. Reinhold and M. Wienecke, J. Cryst. Growth **204**, 434 (1999).

[98] J. L. Merz, H. Kukimoto, K. Nassau, and J. W. Shiever, Phys. Rev. B **6**, 545 (1972).

[99] A E Thomas, G J Russell, and J Woods, J . Phys. C: Solid State Phys. **17**, 6219 (1984).

[100] Yu.V. Korostelin, V.I. Kozlovsky, A.S. Nasibov, and P.V. Shapkin, J. Cryst. Growth **161**, 51 (1996).

[101] D. S. Jiang, H. Jung, and K. Ploog, J. Appl. Phys. **64**, 1371 (1988).

[102] J. M. Noras and J. W. Allen, J. Phys. C: Solid St. Phys. **13**, 3511 (1980).

[103] K.A. Kikoin, V.I. Sokolov, V.N.Flerov, and V.V. Chernyaev, Sov. Phys. JEPT **56**, 1354 (1982).

[104] Z. Zhu *et al.*, Appl. Phys. Lett. **67**, 2167 (1995).

[105] M. L. Reynolds and G. F. J. Garlick, Infrared Physics **7**, 151 (1967).

[106] J. Cisowski, J. Magn. and Magn. Mater. **205**, 323 (1999).

[107] G. Grebe, G. Roussos, and H.-J. Schulz, J. Phys. C: Solid State Phys. **9**, 4511 (1976).

[108] D.D. Nedeoglo, Phys.Stat.Sol. (b) **80**, 369 (1977).

[109] A. Ben Mahmoud *et al.*, Phys. Rev. B **74**, 115203(5p.) (2006).

[110] K. H. J. Buschow and F. R. de Boer, *Physics of Magnetism and Magnetic Materials* (Kluwer Academic Publishers, 2004).

[111] B.I. Shklovskii and A.L. Efros, *Electronic Properties of Doped Semiconductors* (Springer-Verlag, 1984).

[112] David R. Lide (Ed.), *CRC Handbook of chemistry and physics* (CRC Press, 2003), 84th edition.

[113] A.Karipidou, H. Nelkowski, and G.Roussos, J. Cryst. Growth **59**, 307 (1982).

[114] Akihiko Yoshikawa, Hiroshi Nomura, Shigeki Yamaga, and Haruo Kasai, J. Appl. Phys. **65**, 1223 (1989).

[115] J.F. Wang, C.B. Oh, and M. Isshiki, J. Cryst. Growth **297**, 95 (2006).

[116] Qiuchun Sheng *et al.*, J.Lumin. **144**, 26 (2013).

[117] D.D. Nedeoglo, Phys.Stat.Sol. (b) **80**, 369 (1977).

[118] M. Vaziri, Appl. Phys. Lett. **65**, 2568 (1994).

[119] A.L.Gurskii, J. Appl. Spectroscopy **67**, 111 (2000).

[120] Masahiro Orita, Takashi Narushima, and Hiroaki Yanagita, Jpn. J. Appl. Phys. **46**, L976 (2007).

[121] A.R. Hutson, Phys.Rev. **108**, 222 (1957).

[122] P.S. Kireev, *Semiconductor physics* (Mir PublishersMoscow, 1978), p. 693.

[123] *Heavily doped semiconductors*, edited by V.I. Fistul (Plenum PressNew York, 1969), p. 418.

[124] E. Tournie *et al.*, J. Appl. Phys. **80**, 2983 (1996).